Journal of Energy Storage 92 (2024) 111608

Contents lists available at ScienceDirect

Journal of Energy Storage

journal homepage: www.elsevier.com/locate/est

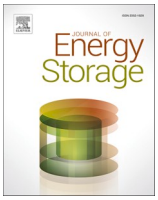

Research papers

Analyzing the melting process in a tilted heat sink filled with a phase change material equipped with the plate and optimized tree-shaped metal fins

Mohamed Boujelbene [a], Hakim S. Sultan [b,c], S.A.M. Mehryan [d,*], Amira M. Hussin [e], Abed Saif Alghawli [f], Mohammad Ghalambaz [g,**]

[a] Industrial Engineering Department, College of Engineering, University of Ha'il, Ha'il 55476, Saudi Arabia
[b] College of Engineering, University of Warith Al-Anbiyaa, Karbala 56001, Iraq
[c] College of Engineering, University of Kerbala, Kerbala, Iraq
[d] Department of Mechanical and Energy Engineering, Shahid Beheshti University, A.C., P.O. Box 16765-1719 Tehran, Iran
[e] Department of Mathematics, Al-Aflaj College of Science and Humanities, Prince Sattam bin Abdulaziz University, Al-Aflaj 710-11912, Saudi Arabia
[f] Department of Computer Science, Al-Aflaj College of Science and Humanities, Prince Sattam bin Abdulaziz University, Al-Aflaj 710-11912, Saudi Arabia
[g] Laboratory on Convective Heat and Mass Transfer, Tomsk State University, 634050 Tomsk, Russia

ARTICLE INFO

Keywords:
Optimized tree-shaped fin
Heat sink
Plate fin
Nano-enhanced phase change material
Electronic device

ABSTRACT

The prevalent practice of integrating metal fins into phase change material (PCM) serves to enhance the thermal conductivity of PCM technology, which finds extensive utility in the efficient heat management of electronic devices. This study delves into the thermal behavior of an inclined heat sink that employs both the optimized tree-shaped and plate fins, each with volume fractions of 20 % and 30 %. The tree-shaped fins underwent optimization using the density-driven topology optimization technique. The heat sinks are loaded with either pure PCM or various types of nano-enhanced PCMs. The study highlights the superior performance of tree-shaped fins in terms of promoting temperature uniformity across the heat sink. It is also found that the performance of tree-shaped and plate designs of metal fins in achieving lower melting times is dependent on the inclination angle of the device. The plate heat sink with a metal volume fraction of 20 % and tree-shaped heat sink with a metal volume fraction of 30 % exhibit, respectively, the highest and the least dependence on the inclination angle in terms of its thermal behavior. Moreover, both the plate and tree-shaped heat sinks demonstrate the quickest complete melting time when the inclination angle is set to 0°. In the tree-shaped heat sink with 20 % and 30 % mass fractions, PCM experiences the longest complete melting time at inclination angles of 75° and 90°, respectively. Furthermore, the most significant reduction in melting time for tree-shaped heat sinks with 20 % and 30 % mass fractions, compared to plate heat sinks, is observed at inclined angles of 30° and 45°. Furthermore, the investigation shows that plate-fin heat sinks experience a more significant enhancement in melting rate due to the presence of diverse nanoparticles. Also, the dispersion of various nano-additives in the PCM within the plate-fin heat sink with a metal mass fraction of 30 % leads to a notable reduction in the maximum temperature of the concentrated heat source (approximately 6.5°C). In contrast, the addition of nano-additives does not have a substantial effect on the maximum temperature for the optimized tree-shaped heat sinks. Finally, upon loading the nanoparticles into the PCM, the plate-fin heat sink with a metal mass fraction of 20 % exhibits the highest temperature non-uniformity within the metal structure, while the tree-shaped heat sink with a metal mass fraction of 30 % shows the lowest.

* Corresponding author.
** Correspondence to: M. Ghalambaz, Laboratory on Convective Heat and Mass Transfer, Tomsk State University, 634050 Tomsk, Russia.
E-mail addresses: Alal171366244@gmail.com (S.A.M. Mehryan), m.ghalambaz@gmail.com (M. Ghalambaz).

https://doi.org/10.1016/j.est.2024.111608
Received 15 October 2023; Received in revised form 10 March 2024; Accepted 4 April 2024
Available online 22 May 2024
2352-152X/© 2024 Elsevier Ltd. All rights reserved.

1. Introduction

Recent increases in the demand for energy-efficient and environmentally sustainable solutions have spurred extensive research and innovation in numerous fields of energy management [1,2]. Phase change materials (PCMs) have emerged as a viable alternative for thermal energy storage applications due to their ability to store energy through latent heat absorption and release, remarkable energy storage capabilities, thermal conductivity, and isothermal behavior during phase transitions [3,4]. However, the naturally limited thermal conductivity of many organic and inorganic PCMs may hinder their efficacy and limit their application in certain circumstances [5]. The numerical investigation conducted by Mallya and Haussener [6] delved into the phenomenon of phase transition occurring within cylindrical encapsulations positioned both horizontally and vertically, featuring a constant temperature wall. This study focused on two distinct PCMs: the commercially accessible paraffin RT27, characterized by low conductivity, and the high-conductivity metal alloy Al-12.6Si. The manipulation of the mushy constant was found to impact solely the melting rate in PCMs with low conductivity, whereas, in PCMs with high conductivity, only the shape of the melt interface was influenced by the mushy constant.

Incorporating metal structures, which can function as thermal conduits and improve overall efficiency, is a practical strategy for enhancing heat transfer in PCM systems [7,8]. In addition, incorporating metal fins or porous metals into PCMs has become a popular method for augmenting the overall heat transfer in latent heat thermal energy storage (LHTES) systems, primarily due to their exceptional thermal efficiency [9]. To maximize the efficacy of LHTES systems, researchers have investigated a variety of fin designs in recent years. The majority of these studies have focused on the geometry of the fins, with longitudinal and radial fins in cylinder-shaped PCM enclosures being the most prevalent varieties. In addition to these conventional fin configurations, there has been an increase in innovative fin designs, which have demonstrated greater heat transfer capabilities in PCMs than in their conventional counterparts [10].

Through the use of metallic protrusions such as fins, it is possible to improve thermal exchange between the dynamic barrier and PCMs. This allows heat to permeate the PCM effectively. The design of these fins depends on the surface to which they will be affixed. Radial, axial, or helical fins are appropriate for tubular and cylindrical structures, whereas linear fins are required for flat surfaces. Due to ongoing advancements in computational fluid dynamics simulation software, a number of analytical studies [10–12] have investigated complex fin configurations and varying layouts to optimize thermal efficiency. Fakhar [13] investigated the enhancement of melting and solidification processes of nano-enhanced PCM (NePCM) in a horizontally arranged latent heat thermal energy storage unit using branched-fin designs and nanoparticles. Three proposed five-fin designs are contrasted with a Y-oriented triple-fin design. The research indicates that a double-branched or leaf-vein pattern performs the best, dissolving 1.85 times faster than the basal case. In addition, increasing nanoparticle concentration enhances melting and solidification rates while decreasing energy storage with increasing concentration. Moreover, in comprehensive reviews, Teggar et al. [7] and Zhang et al. [10] addressed various types of fins utilized in thermal energy storage units. The straight fins [14–17], longitudinal fins [18,19], and radial fins [20] have been investigated for thermal energy storage and phase change heatsinks.

Li et al. [21] investigated the use of PCMs within a shell-and-tube TES system with leaf-shaped longitudinal fins. The effects of fin length, angle, and material on melting efficacy were subsequently investigated and discussed. Two alternative configurations, rectangular and triangular sub-branches, were examined to evaluate the effect of leaf-fin shape on the PCM melting process. The investigation reaches the following conclusions. The biomimetic design of the leaf-shaped fin, with its gradually increasing sub-branch lengths, provided an additional thermal contact surface for PCM further from the heating source, facilitating uniform heat transmission and faster melting. The largest heat transfer surface was provided by a 75° branch angle, which increased the contact area between the fin and PCM, resulting in the maximum melting rate. Compared to a 90° branch angle, the total melting time was decreased by 13 %. The total melting time was reduced by 14.2 % when the fin length was increased from 22mm to 25mm, resulting in a 16.9 % increase in charging capacity.

The tree-shaped fins have been used in very few studies. Some studies investigated non-branching fins. Skaalum and Groulx [22] examined the heat transmission between bifurcated and straight fins in latent heat energy storage systems. These systems can increase energy density and quality, but their limited thermal conductivity frequently necessitates enhanced heat exchanger designs. Due to limited convective cell formation, bifurcated fins transferred less energy during charging but provided a more consistent, albeit lower, heat transfer rate during discharging. Bifurcated fins offer no significant benefits in a shell-and-pipe energy storage system, despite their slightly increased energy exchange over 8 h. In another study, Duan et al. [23] explored the melting rates of PCMs in honeycomb structures with different geometrical components in an effort to identify the optimal shape for reducing melting time. It focuses on the influence of shape, aspect ratio, and orientation on paraffin melting rates in honeycomb, circular, triangular, hexagonal and quadrilateral cores. The results indicate that rectangular cores consistently outperform hexagonal cores in terms of melting rate, with geometrical factor, emerging as a key indicator of melting rate. In terms of disintegration rate, hexagonal cells are not the optimal solution for honeycomb centers.

Ho et al. [24] employed a topology optimization (TO) approach to construct innovative, improved structures. A comprehensive numerical investigation investigates the impact of different thermal transport mechanisms on TO design for both steady-state and transient heat conduction with phase change. The tree-like structure of the TO-generated heat sink was fabricated using selective laser melting (SLM), an additive manufacturing technique for metals, to facilitate production and performance evaluation. Trials conducted on three specific PCMs (RT35, RT35HC, and RT44HC) with heat flux variations from $4kW/m^2$ to $7.24kW/m^2$ demonstrated that the tree-inspired TO heat sink is superior to traditional fin-designed heat sinks, recording up to 4 °C cooler wall temperatures. For medium heat flux levels, RT35HC shows the best thermal behavior, whereas RT44HC is most efficient at higher heat fluxes. With the tree-like configuration, operating durations can be increased by as much as 13 % in comparison to finned heat absorbers [24]. The heat sink's tree-mimicked design boasts superior thermal capabilities due to the fine-tuned heat conduction routes which ensure heat is transferred efficiently from the source to the PCM. The findings from this study highlight the efficacy of TO PCM-based heat sinks in improving electronic cooling and offer insightful pointers for crafting and deploying TO configurations in diverse cooling scenarios.

Low heat transfer and the lack of free convection limit the phase change rate of PCM in microgravity environments, such as spacecraft operations. It is proposed to incorporate fractal tree-like blades into to accelerate melting in microgravity. Using a transient enthalpy-porosity-based model, the heat transmission behavior of cavities with tree-like fins at 30°, 60°, and 90° bifurcation angles are investigated. The results indicate that tree-like fins accelerate melting in conjunction with heat conduction and thermocapillary convection, with larger bifurcation angles resulting in quicker melting rates. Compared to finless cavities, melting durations are reduced by 47.7 %, 57.2 %, and 64.3 % for 30°, 60°, and 90° fins, respectively. Moreover, the fractal-inspired tree-like fins amplify energy storage potential and initially boost heat transfer during the melting phase, though there's a slight reduction towards the conclusion. The effect of thermocapillary convection on melting in microgravity increases as the bifurcation angle increases.

Innovative tree-like appendages can be used to regulate the temperature of spacecraft electronic devices [25]. Xie et al. [26] analyzed

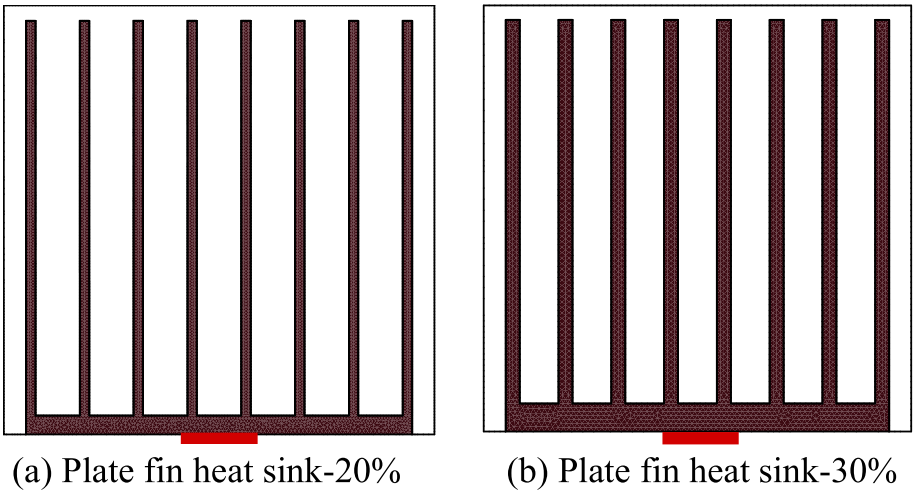

Fig. 1. Plate-fin heat sinks (PS) with metal volume fraction of (a) 20 %, and (b) 30 %.

the thermal attributes of a PCM-integrated heat sink, comparing innovative dendritic conductive designs to traditional plate fin configurations, concentrating on the role of natural convection using numerical simulations. Research indicated that the impact of natural convection varies based on the orientation, structure, and volume ratio of the metal, with the orientation being the most influential factor. The optimized tree-shaped structure promoted natural convection, thereby improving heat transfer, thermal blending, and fin efficiency. Improving heat conduction and restricting convection flow reduced the effect of natural convection as the volume fraction of metal increased. The optimized tree-shaped structure is suitable for applications that require minimally conductive material and substantial natural convection. Recent research has highlighted the efficacy of tree-like fin designs in boosting heat transfer within PCMs used in LHTES systems. These fins, mirroring natural branching, expand the area available for thermal exchange, thus optimizing PCM thermal management. One study [27] applied entransy theory to refine these fin structures in metal hydride beds, enhancing the output rate of thermal energy significantly. This optimization yielded a notable 11.5 % rise in efficiency compared to standard designs. Another research [28] examined tree-like fins in a NePCM-based heat exchanger, integrating copper nanoparticles to improve conductivity, which cut down the PCM melting time by up to 75.7 %. Additionally, a numerical analysis [29] employed fractal tree-shaped convergent fins in LHTES, adjusting various parameters to decrease PCM solidification time by as much as 12.42 %. These studies collectively underscore the potential of tree-shaped fins in elevating PCM heat transfer efficiency, vital for designing advanced, eco-friendly thermal storage systems.

Khedher et al. [30] investigated the effect of materials and the shape of fins, specifically optimized tree-shaped and simple plate fins in a solid-solid nanocomposite-PCM. Aluminum and copper fins provide the maximum melting rates, while optimized tree-shaped fins show better performance compared to the plate structure fins. The structure's height plays an important role in heat transfer, particularly for highly conductive materials. However, the nanoparticle fraction does not affect the PCM's thermal behavior. Xie et al. [31] investigated the thermal performance of PCMs in a compact thermal energy storage panel with optimized fin structures, which were constructed using a topological structure optimization method. Comparing optimized fin designs to conventional plate fin structures reveals that optimized fins substantially improve PCM melting with the same metal volume fraction. The optimized fin structures offer a more efficient design for high-performance thermal energy storage units while minimizing the amount of thermally conductive material.

Xie et al. [32] focused on elevating the thermal conductance of PCM enclosures for the thermal regulation of portable gadgets using a structure optimization approach based on density. Their research juxtaposed two conventional plate fin heat sink PCM enclosures with metal volume fractions of 20 % and 30 % against dendritic designs having corresponding metal volume fractions of 18.7 % and 27.5 %. By employing the Volume of Fluid and enthalpy-porosity techniques, the study delves into the evolving thermal dynamics of the PCM enclosures. Their findings underscored that the refined dendritic configurations surpass the standard designs, achieving cooler heat source temperatures and more considerable melt proportions during the initial PCM melting phase. A hike in the metal volume fraction bolsters the overall thermal conveyance while reducing temperature disparities. The superior heat transmission performance of upward-oriented PCM enclosures is a result of enhanced thermal mingling from intensified convection movements. The tree-shaped designs provide greater temperature uniformity and lower heat source temperatures than the plate fin designs. The study of Xie et al. [32] demonstrates the viability of using optimization of topological heat conduction structures for thermal management in mobile electronics.

This literature review underscores the pivotal role of fin optimization in advancing heat transfer for thermal energy storage applications. Notably, studies [26,32] have identified tree-shaped fin geometries as the most efficient design, which were subsequently employed in [30]. Building upon these findings, the present study seeks to extend this knowledge by exploring the influence of using nanoparticle additives and tilting the enclosure on the energy storage and heat transfer behavior of optimal tree-shaped fin geometries for the first time.

2. Mathematical model

2.1. Description of plate-fin heat sink

In the ongoing investigation, Fig. 1 presents the heat regulation approach for an electronic apparatus that employs a particular PCM. The suggestion is to utilize a container containing paraffin wax-based PCM, measuring $100mm \times 100mm$ in size, to assimilate the heat emitted by an electronic apparatus. The apparatus, acting as a focused heat source, measures 15 mm in length, with a heat production rate of $50kW/m^2$. Presently, there exist methods accessible to facilitate the dispersion of heat from the heat source to PCM. These techniques entail using customary aluminum plate-fin heat sinks. As shown in Fig. 1(a) and (b), the plate fins have metal volume fractions of either 20 % or 30 % throughout the entire enclosure. The configuration of plate-fin heat sink architectures has been fine-tuned to ensure uniform spacing of the fins within the PCM containers.

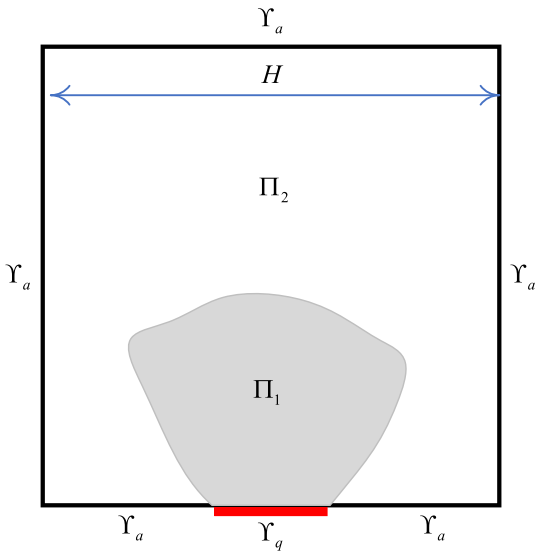

Fig. 2. Visualization of the design domain for two-dimensional heat conduction topology optimization.

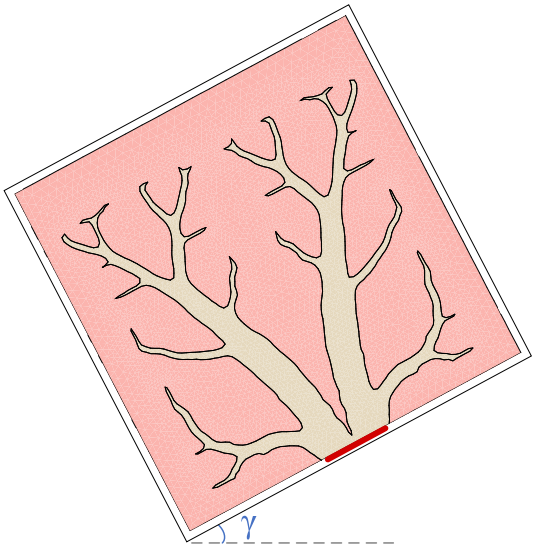

Fig. 4. The inclination angle of the heat sink.

2.2. Topology optimization of heat sink

The design domain takes the form of a square enclosure with a dimension of H. Given that heat transport between the concentrated heat source and the design domain is mainly via diffusion, the temperature distribution within the domain is dictated by Eq. (1). In this equation, Q_{gen} represents a constant heat generation rate per unit volume, exclusively applied within the PCM subdomain. The boundaries of the domain are represented by Υ_a and Υ_q, both of which follow the Newman boundary conditions, as indicated in Eqs. (2) and (3). Therefore, all boundaries are presumed to be insulated, except for a segment of the lower boundary where a constant heat flux is applied. As shown in Fig. 2, the computational domain (Π) comprises two distinct subdomains—one characterized by high thermal conductivity (Π_1) and the other by low thermal conductivity (Π_2). The material selected for this study with high thermal conductivity is an aluminum alloy, identified as λ_1, featuring a thermal conductivity of around 200 $Wm^{-1}K^{-1}$. On the flip side, PCM was employed, characterized by a significantly lower thermal conductivity denoted as λ_2, measuring at 0.2 $Wm^{-1}K^{-1}$. It is worth highlighting that λ_1 is three orders of magnitude higher than λ_2.

$$\nabla.(\lambda\nabla\theta) + Q_{gen} = 0 \quad (1)$$

Table 1
Thermal and physical characteristics of the PCM and solid Aluminum [37,38]

Properties	PCM	Aluminum	Unit
$\rho_{PCM,s}$	880	2710	kgm^{-1}
$\rho_{PCM,l}$	770	–	kgm^{-1}
c_p	2000	897	$Jkg^{-1}K^{-1}$
λ_s	0.2	202	$Wm^{-1}K^{-1}$
λ_l	0.2	–	$Wm^{-1}K^{-1}$
h_{PCM}	125	–	$kJkg^{-1}$
θ_{mel}	35	–	$^{\circ}C$
$\theta_{solidus}$	34	–	$^{\circ}C$
$\theta_{liquidus}$	36	–	$^{\circ}C$

Table 2
Details of mesh cases when $\gamma = 45^{\circ}$.

Case	Triangles		Quads	Computational time
	Fin	PCM		
A	12,360	34,881	5182	13 h 21 min
B	15,101	37,093	5182	17 h 5 min
C	**36,218**	**106,946**	**8680**	**40 h 0 min**
D	54,102	164,174	11,572	65 h 10 min

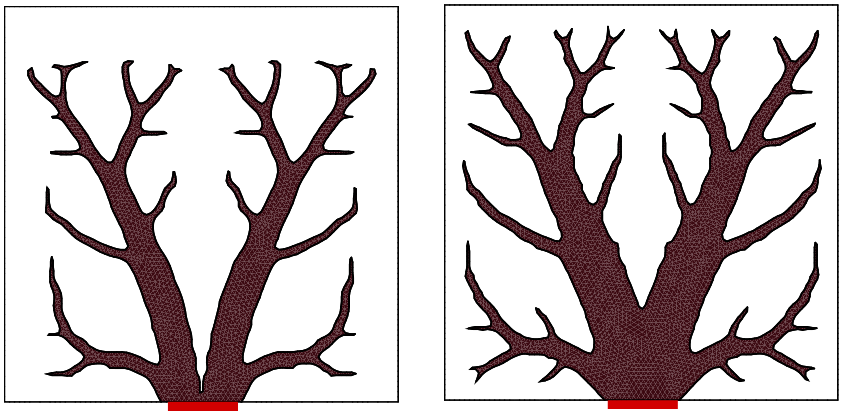

Fig. 3. Heat sink with the optimized tree-shaped fins (TS) with metal volume fraction of (a) 20 %, and (b) 30 %.

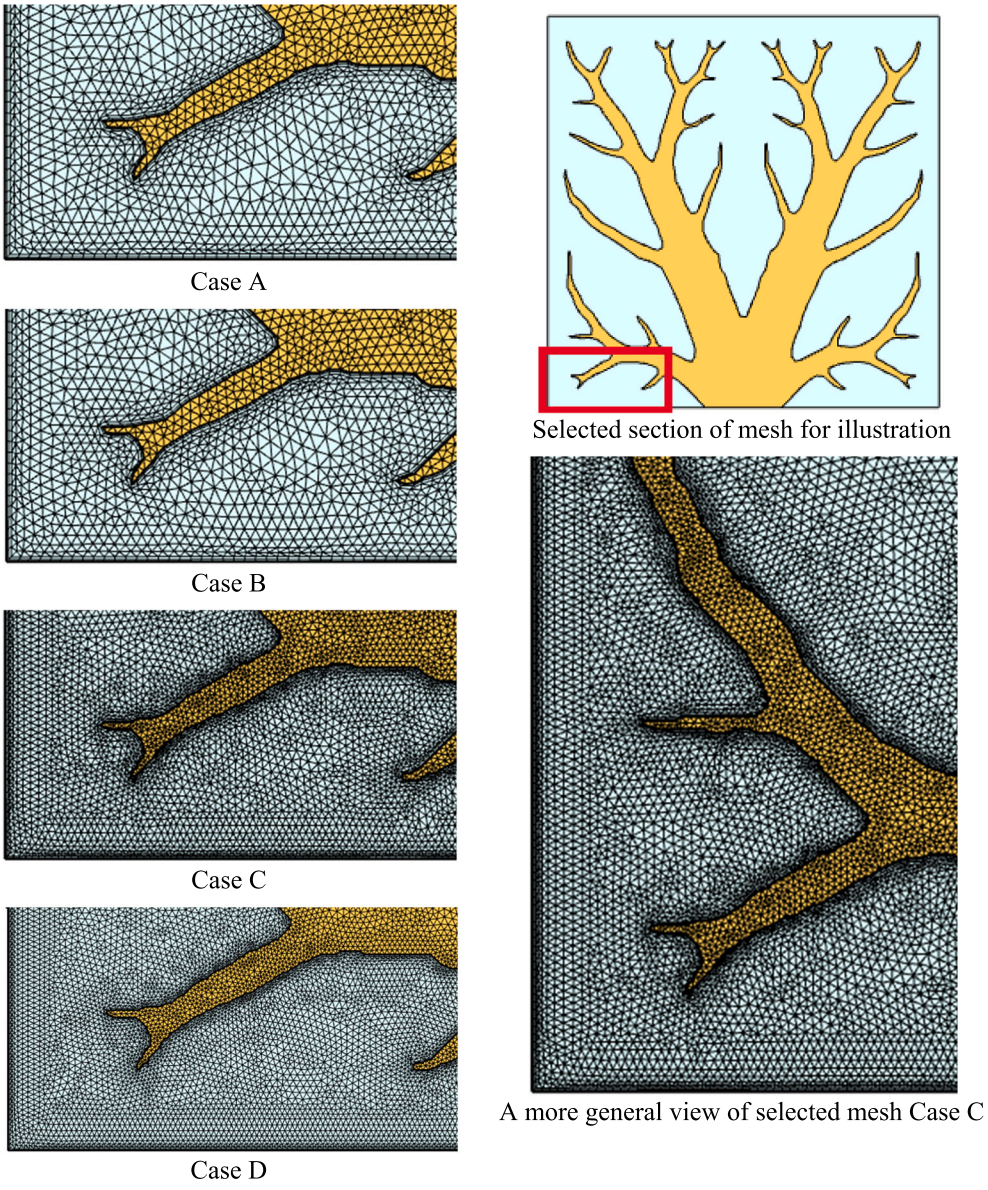

Fig. 5. A view of adopted meshes for case A–D when $\gamma = 45^{\circ}$.

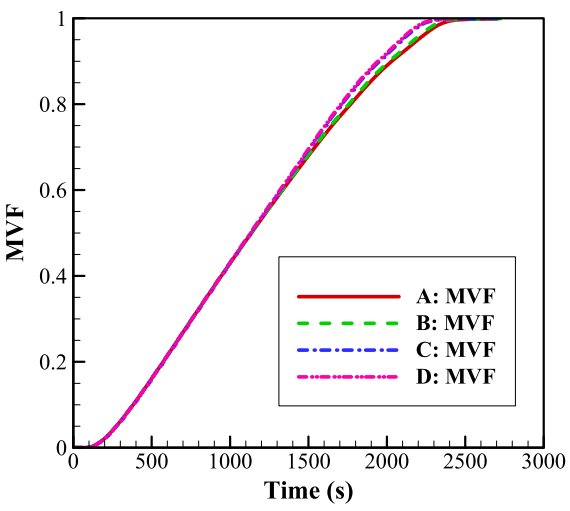

Fig. 6. Impact of mesh resolution on the MVF when $\gamma = 45^{\circ}$.

$$\nabla\theta.\boldsymbol{n} = q^{'} \; on \; \Upsilon_q \tag{2}$$

$$\nabla\theta.\boldsymbol{n} = 0 \; on \; \Upsilon_a \tag{3}$$

The objective of this optimization problem is to craft a conductive heat spreader with the primary goal of augmenting the diffusion-based heat transport between the domain and the boundary subjected to a constant heat flux. To maintain a balanced heat rate within the design domain, an artificial heat source term is incorporated on the right-hand side of Eq. (1) to emulate the heat absorbed by the PCM during the phase change process. The goal of design is to discover the most efficient arrangement of materials, aiming to reduce the overall temperature distribution throughout the domain. Building on prior research [33–35], we utilize the thermal compliance of Eq. (4) as the objective function (*of*) to be minimized. This objective is subject to the constraint of limiting the volume fraction of high thermal conductivity material (Φ_1), as described in Eq. (5). In this equation, ϑ represents the design variable for the two materials, capable of assuming any value within the range of 0 to 1, as depicted in Eq. (6).

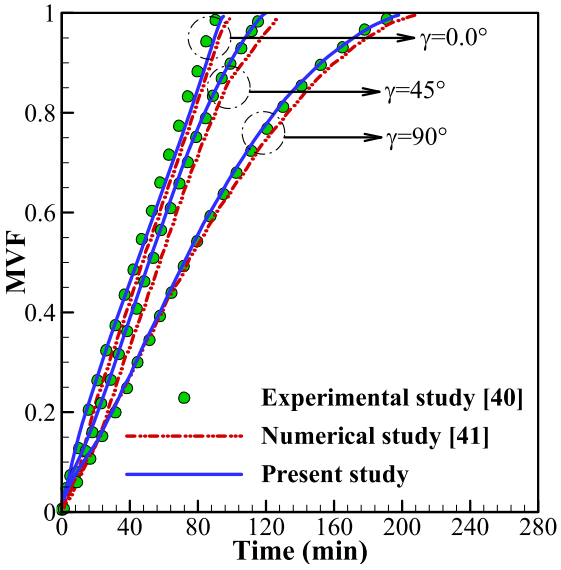

Fig. 7. Melted volume fraction of the present study and that measured by Kamkari et al. [40,41] at different inclination angles.

$$Minimize: of(\vartheta) = \int \nabla\theta(\lambda(\vartheta)\nabla\theta) \tag{4}$$

$$\text{Subject to}: \frac{\int \vartheta dA}{\int dA} \leq \Phi_1 \tag{5}$$

$$0 \leq \vartheta \leq 1 \tag{6}$$

The thermal conductivity parameter (λ) in Eqs. (1) and (4) is expressed as a function of ϑ, where $\vartheta = 1$ corresponds to the thermal conductivity of the aluminum alloy ($\lambda = \lambda_1$), and $\vartheta = 0$ signifies the thermal conductivity of the PCM ($\lambda = \lambda_1$). However, to facilitate numerical solutions and mitigate challenges associated with discrete design variables of 0 and 1, we employ the Solid Isotropic Material with Penalization (SIMP) method. The SIMP method adopts a density-based approach, substituting discrete variables with continuous values. The method incorporates a power-law interpolation function designed to penalize intermediate values (those falling between 0 and 1) and guide the solution towards the extremes of 0 and 1. Employing the SIMP method involves replacing the λ terms in Eqs. (1) and (4) with the formulation provided in Eq. (7), where a penalization factor (*pf*) of 3 is utilized. Likewise, given that the term Q_{gen} is exclusively applied within the PCM domain, an interpolation function for Q_{gen}, as defined in Eq. (8), has been introduced. In this equation, C represents a constant with a value of 10^{-8}, and $Q_{gen,max}$ denotes the maximum volumetric heating rate, maintained as a constant. Examining Eq. (8), it is evident that in the aluminum domain ($\vartheta = 1$), $Q_{gen}(\vartheta)$ is approximately 0, whereas in the PCM domain ($\vartheta = 0$), $Q_{gen}(\vartheta)$ approximates $Q_{gen,max}$. In a manner akin to the SIMP method applied for thermal conductivity interpolation, we employ a penalization factor (*pf*) of 3 in Eq. (8). Ultimately, volume constraints of 0.2 and 0.3 are imposed for Φ_1.

$$\lambda = \lambda_2 + \vartheta^{pf}(\lambda_1 - \lambda_2) \tag{7}$$

$$Q_{gen}(\vartheta) = Q_{gen,max}\left[\left(1 - \vartheta^{pf}\right) + C\vartheta^{pf}\right] \tag{8}$$

The solution to the topology optimization problem was achieved through the application of the COMSOL Multiphysics software version 5.6. It is important to highlight that in the topology optimization simulation, convergence was considered achieved when all constraints were satisfied, and the relative change in the compliance objective was less than 10^{-3}. The illustrations in Fig. 3(a) and (b) portray the heat sinks that have been designed using the topological optimization technique.

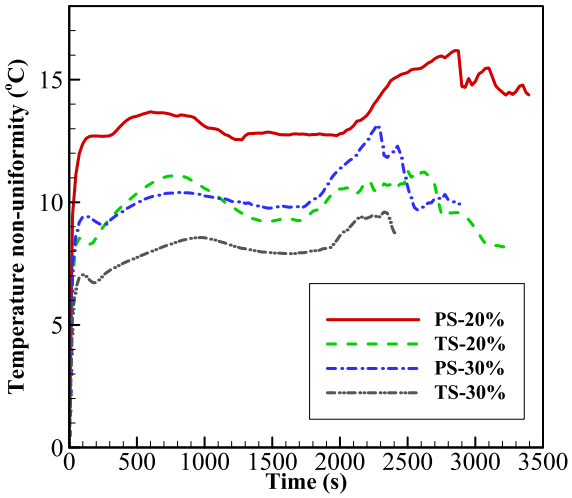

Fig. 9. Temperature non-uniformity of fins with different designs when $\gamma = 45^{\circ}$.

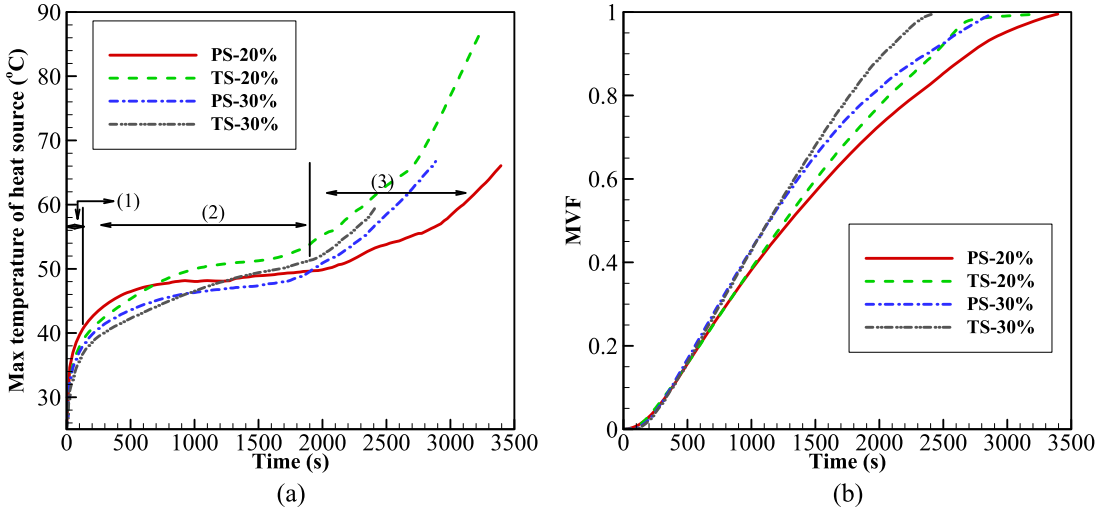

Fig. 8. (a) Maximum temperature of heat source, and (b) normalized melted volume fraction for different designs of heat sink when $\gamma = 45^{\circ}$.

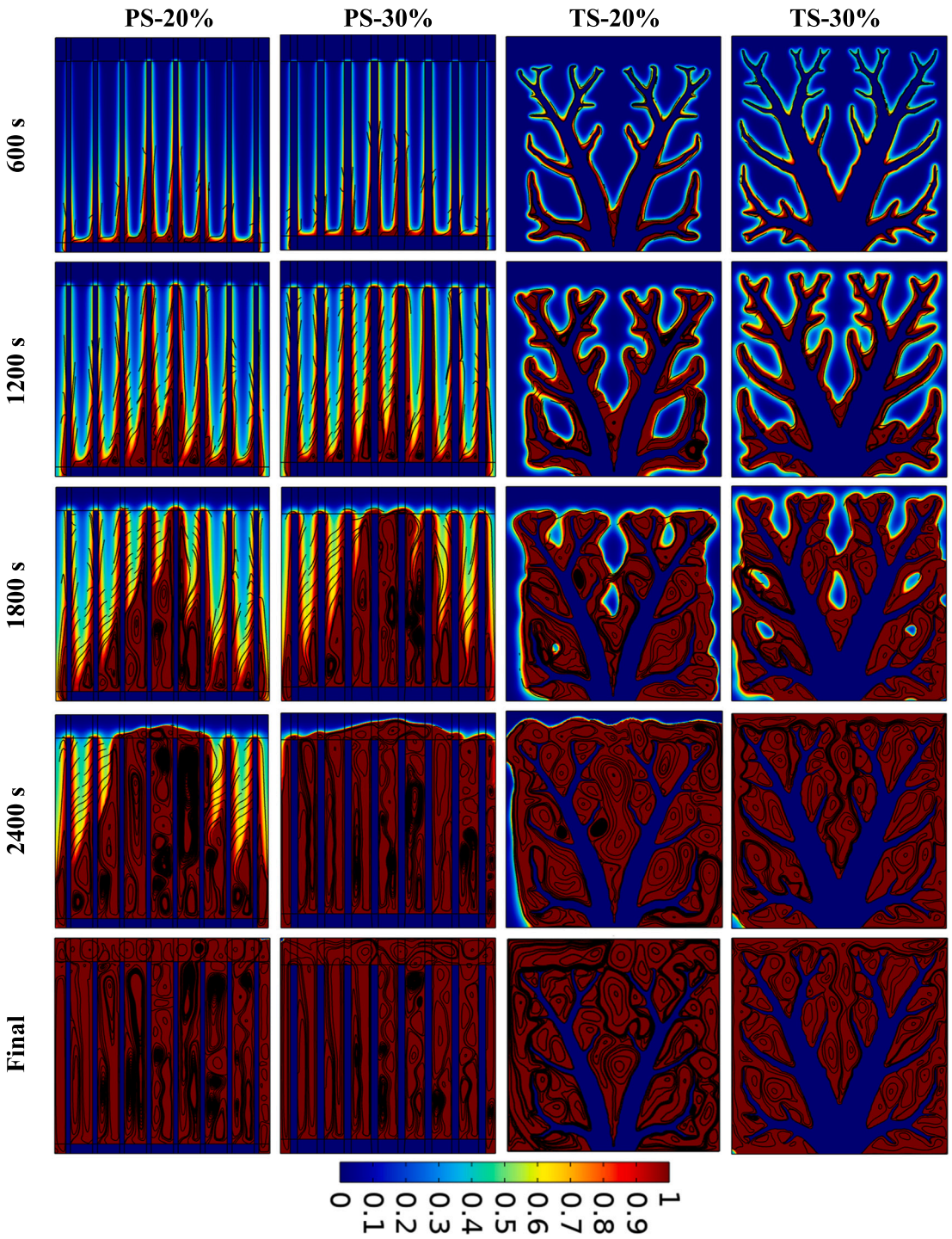

Fig. 10. Phase change interface and streamlines at various time snaps when $\gamma = 45^{\circ}$.

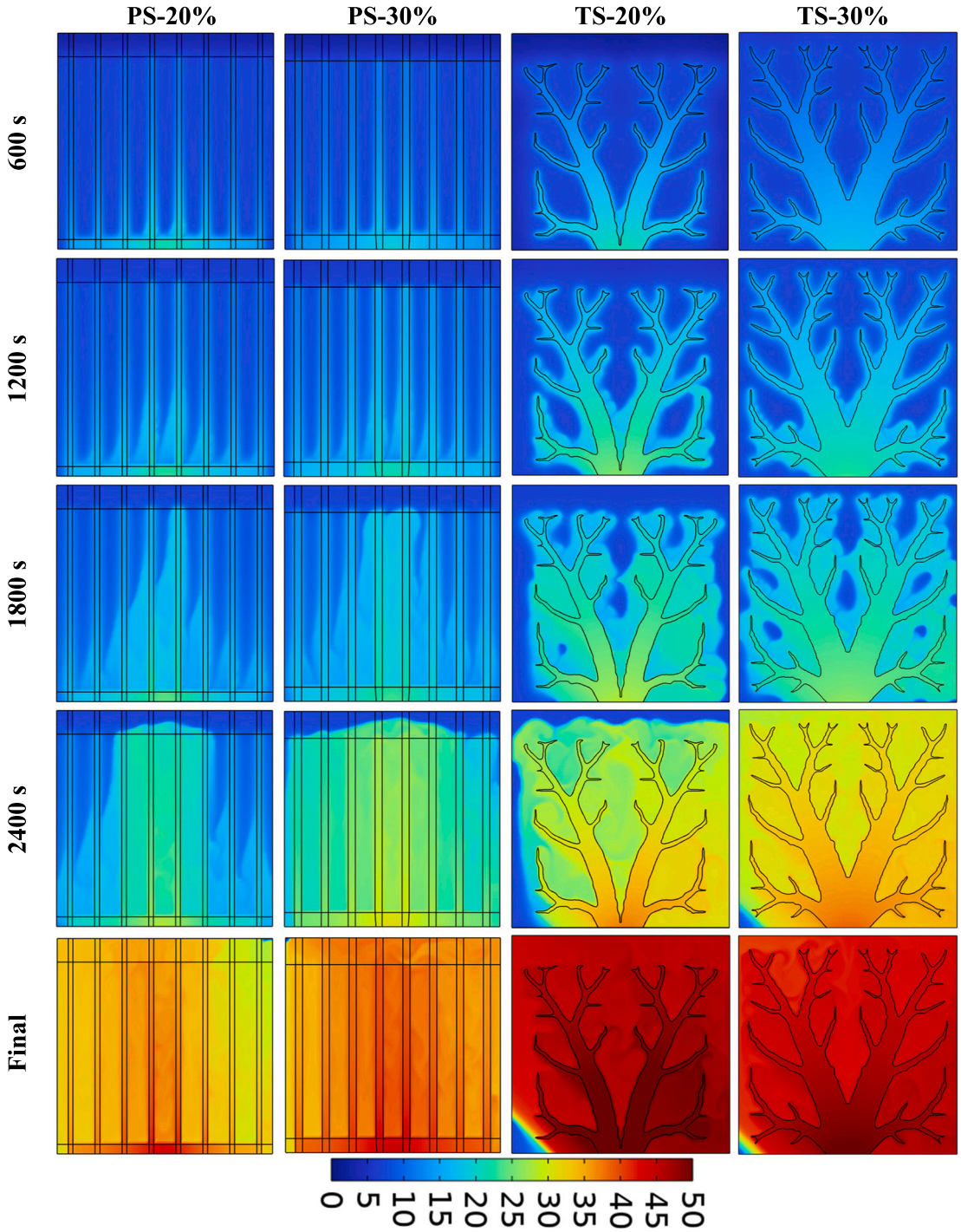

Fig. 11. Isotherms for $(\theta - \theta_c)$ at various time snaps during the melting process when $\gamma = 45^{\circ}$. Temperature higher than $50^{\circ}C$ is depicted the same as $50^{\circ}C$.

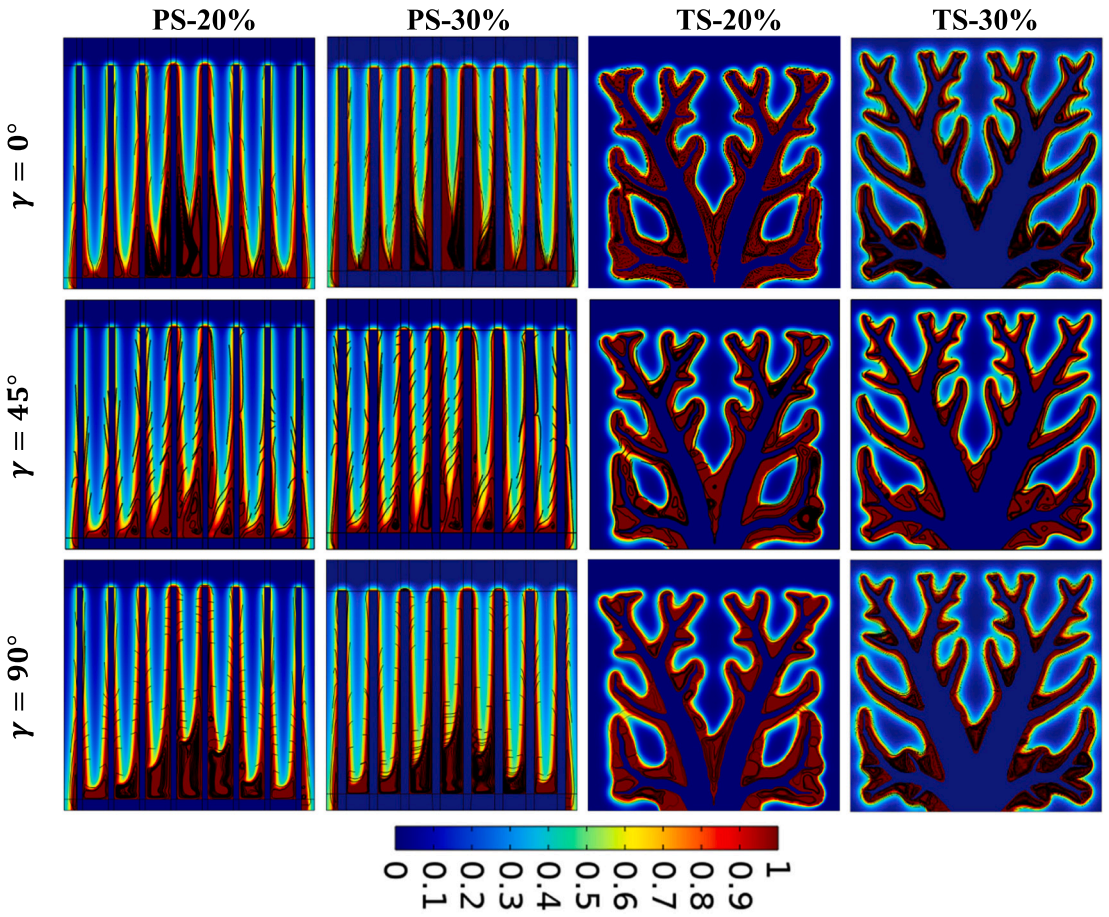

Fig. 12. Phase change interface and streamlines at various inclination angles at $t = 1200\ s$.

2.3. Modeling the melting process in the heat sink

In order to model the melting front that involves the solid-liquid interface, the study utilized the enthalpy-porosity approach. In this approach, the entirety of the computational domain is treated as a porous medium, exhibiting variable porosity values spanning the range from zero to one. In the area where the PCM is entirely liquified, the porosity attains a value of one. Conversely, within the sub-domain where no melting has occurred, the porosity is established at zero. The region between the two completely melted, and solid regions is called the mushy zone, with a porosity varying between zero and one [15,26,36].

I) Mass conservation

$$\nabla \cdot u = 0 \tag{9}$$

II) Momentum equations

$$\rho_{PCM,l}\frac{\partial u}{\partial t} + \rho_{PCM,l}(u\cdot\nabla)u = \nabla\cdot\left[-pI + \mu_{PCM,l}\left(\nabla u + (\nabla u)^T\right)\right] + (\rho\beta)_{PCM,l}g_i(\theta - \theta_{mel}) + F(\theta)u \tag{10}$$

in which,

$$F(\theta) = A_{mush}\frac{1-2\ell(\theta)+\ell^2(\theta)}{\Gamma+\ell^3(T)}; A_{mush} = 5\times10^5 \text{ and } \Gamma = 10^{-3} \tag{11}$$

and

$$g_i = \begin{cases} g\sin\gamma & i = x \\ g\cos\gamma & i = y \end{cases} \tag{12}$$

in which γ is the angle of inclination of the enclosure (Fig. 4).

To derive the properties of PCM within the mushy region, a method is utilized that revolves around approximating through the use of piecewise polynomials.

$$\ell(\theta) = \begin{cases} 0 & \theta \le \theta_{mel} - \dfrac{\Delta\theta_{mel}}{2} \\ \dfrac{\theta-\theta_{mel}}{\Delta\theta_{mel}} + \dfrac{1}{2} & \theta_{mel} - \dfrac{\Delta\theta_{mel}}{2} < \theta < \theta_{mel} + \dfrac{\Delta\theta_{mel}}{2} \\ 1 & \theta \ge \theta_{mel} + \dfrac{\Delta\theta_{mel}}{2} \end{cases} \tag{13}$$

in which, $\Delta\theta_{mel}$ $\left(\text{i.e.}, \theta_{liquidus} - \theta_{solidus}\right)$ is $2^{\circ}C$.

III) Energy conservation for the PCM

$$\left(\rho c_p\right)_{PCM}\frac{\partial\theta}{\partial t} + \left(\rho c_p\right)_{PCM,l}\vec{U}.\nabla\theta = \nabla.(\lambda_{PCM}\nabla\theta) - \rho_{PCM}h_{PCM}\frac{\partial\ell(\theta)}{\partial t} \tag{14}$$

in which,

$$\left(\rho c_p\right)_{PCM} = \ell(\theta)\left[\left(\rho c_p\right)_{PCM,l} - \left(\rho c_p\right)_{PCM,s}\right] + \left(\rho c_p\right)_{PCM,s} \tag{15}$$

$$\rho_{PCM}(\theta) = \ell(\theta)\left(\rho_{PCM,l} - \rho_{PCM,s}\right) + \rho_{PCM,s} \tag{16}$$

$$(\lambda)_{PCM}(\theta) = \ell(\theta)\left[(\lambda)_{PCM,l} - (\lambda)_{PCM,s}\right] + (\lambda)_{PCM,s} \tag{17}$$

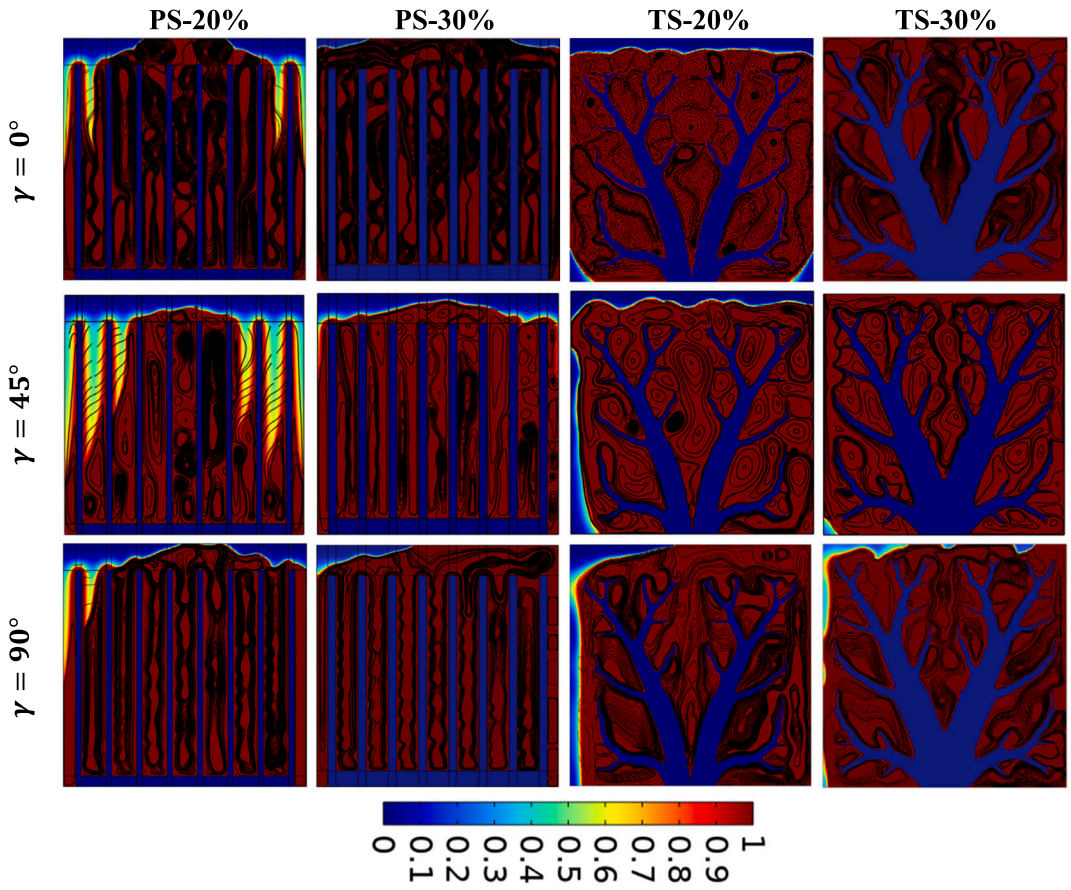

Fig. 13. Phase change interface and streamlines at various inclination angles at $t = 2400\ s$.

IV) Energy conservation for the fin

$$(\rho c_p)_{fin}\frac{\partial\theta}{\partial t} = \nabla.(\lambda_{fin}\nabla\theta) \tag{18}$$

The boundary and initial conditions imposed on the physical domain are as the following:

At the outer walls:

$$u = v = 0, \left.\frac{\partial\theta}{\partial n}\right|_{PCM} = 0 \tag{19}$$

At the walls of the fin:

$$\theta|_{fin} = \theta|_{PCM}, \lambda_{fin}\left.\frac{\partial\theta}{\partial n}\right|_{fin} = \lambda_{fin}\left.\frac{\partial\theta}{\partial n}\right|_{PCM} \tag{20}$$

At the root of the tree-shaped fin.

$$\lambda_{fin}\left.\frac{\partial\theta}{\partial n}\right|_{fin} = q^{'} = 50\frac{KW}{m^2} \tag{21}$$

To model the behavior of the PCM domain, we need to establish the initial condition. Specifically, we can express the initial condition as follows

$$u = v = 0, \theta|_{PCM} = \theta_{initial} = 25^{\circ}C \tag{22}$$

It is worth noting that the metal fins are made of Aluminum 6010. To account for temperature-dependent changes in the dynamic viscosity of the liquid PCM, the simulation employs a method for estimating the viscosity as a function of temperature. Specifically, the dynamic viscosity is calculated using the following approach:

$$\mu_{PCM,l} = 0.001e^{C_1 - \frac{C_2}{\theta_{PCM,l}}} \tag{23}$$

in which C_1 and C_2 are, respectively, −4.25 and −1790 [20]. The thermophysical properties of the PCM and aluminum are presented in Table 1.

The melting volume fraction refers to the fraction of the total volume of a material that has melted. This can be assessed by dividing the volume of the liquefied material by the overall volume of the substance. Mathematically, the melting volume fraction can be expressed as:

$$MVF(t) = \frac{\int_{\forall}\ell(\theta)d\forall}{\int_{\forall}d\forall} \tag{24}$$

The temperature non-uniformity of a fin pertains to the temperature variation across the fin's surface and is commonly computed as the disparity between the highest and lowest temperatures exhibited by the fin. This temperature difference is an important parameter to consider when designing and optimizing fins for heat transfer applications, as a high-temperature non-uniformity can lead to local hot spots that may cause thermal stress or reduce the overall effectiveness of the fin.

3. Solution approach

3.1. Numerical approach

Employing the finite element method (FEM) is a robust strategy when addressing the challenge of solving complex partial differential equations (PDEs). This encompasses equations that describe fundamental physical quantities like momentum, mass, and energy. By dividing the domain into small elements and approximating the solution

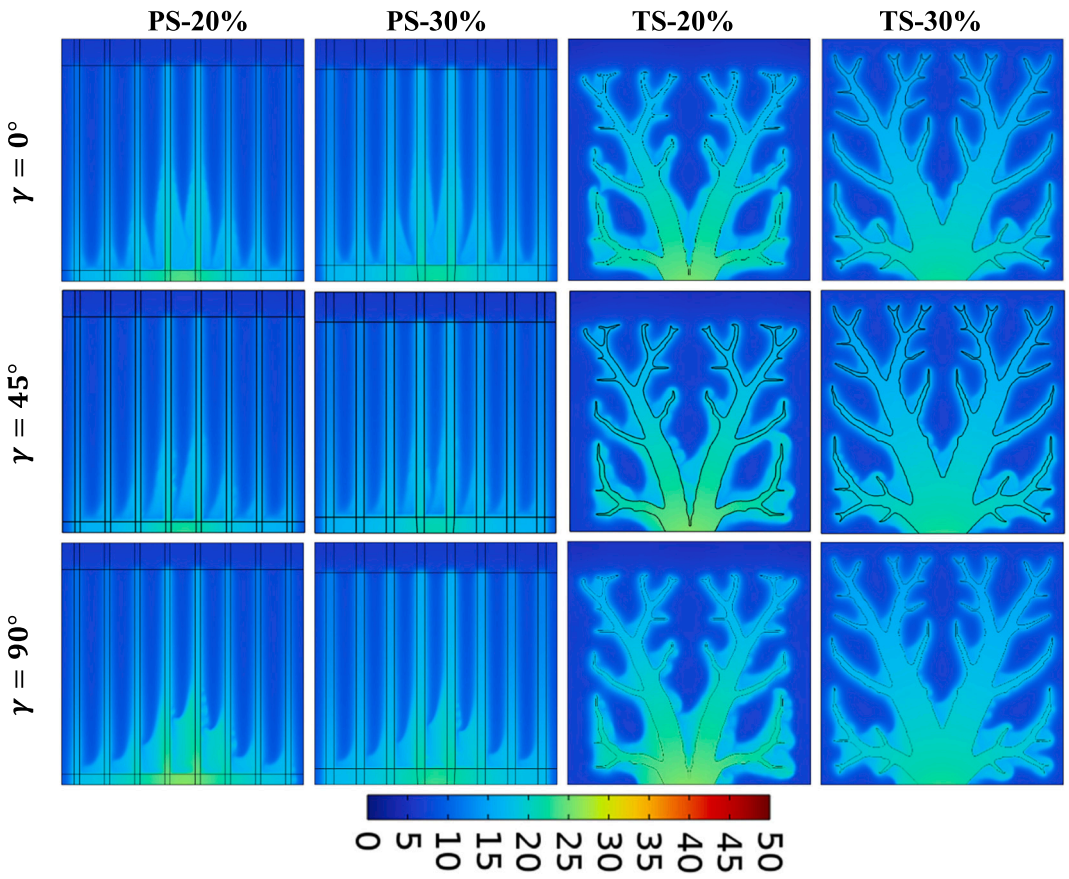

Fig. 14. Isotherms for $(\theta - \theta_c)$ at various inclination angles at $t = 1200\,s$. Temperature higher than $50^{\circ}C$ is depicted the same as $50^{\circ}C$.

using basis functions, the FEM provides an efficient and accurate method for computing the behavior of physical systems. In this approach, the governing equations are transferred to the weak form. The formulation of the weak form of a PDE involves multiplying the PDE by a weight function and subsequently integrating it across the domain. This process is also known as Galerkin's method. The weak form of a PDE is typically more amenable to numerical approximation than the strong form. This is because the weak form involves only first-order derivatives, whereas the strong form involves second-order derivatives. The weak form also allows us to apply a wider range of boundary conditions than the strong form. The approach of Gauss quadrature integration was utilized to combine the equations across the elements and produce a set of algebraic residual equations. To achieve convergence, the residual equations were iteratively solved through a coupled use of the PARDISO solver with the aid of the Newton method. To optimize the convergence of the algorithm, a damping factor of 0.8 was applied. In order to maintain solution accuracy below a relative threshold of 10^{-4}, the time step was regulated using the backward differential formula [39], with an adaptable order ranging from 1 to 2. This approach enabled the algorithm to maintain accuracy while also allowing for adaptability in response to changing conditions.

3.2. Grid study

Grid studies are essential in numerical investigations as the accuracy and efficiency of the numerical method heavily depend on the grid configuration. A poorly chosen grid configuration can lead to inaccurate or inefficient solutions, while an optimal grid configuration can significantly improve the accuracy and efficiency of the method. Therefore, grid studies are used to ensure that the numerical method produces reliable and accurate results. To achieve a mesh optimal in this study, the optimized tree-shaped fin with the volume fraction of 30 % aluminum under the skew angle of 45° relative to the horizontal axis is selected. As shown in Table 2, four different cases with varying numbers of elements have been utilized to discretize the computational domain for numerical analysis. Fig. 5 is a representation of the employed meshes for case A-D when $\gamma = 45^{\circ}$. As can be seen from Fig. 6, considering the equilibrium between precision and computational expenses, Case C was selected for computations.

3.3. Validation and verification

The validity of the current theoretical model and numerical simulation will be assessed by comparing our results to relevant experimental and numerical data found in the literature [40,41]. Kamkari et al. [40,41] investigated the melting behavior of lauric acid within an inclined rectangular capsule using both numerical and experimental approaches. The rectangular capsule used in the study has dimensions of 5 *cm* (width) and 12 *cm* (height). One of the walls of the enclosure, the right wall, was held at $70^{\circ}C$. The other walls were thermally insulated to inhibit heat transfer. Herein, to validate the tilted-angle computations, three different inclination angles of the enclosure are simulated. Fig. 7 illustrates a comparison between the volume fraction of melted lauric acid obtained from the present study and those reported by Kamkari et al. [41] for three inclination angles of enclosure. The results obtained from our study exhibit a notable level of agreement with those reported by Kamkari et al., as can be observed from the comparison.

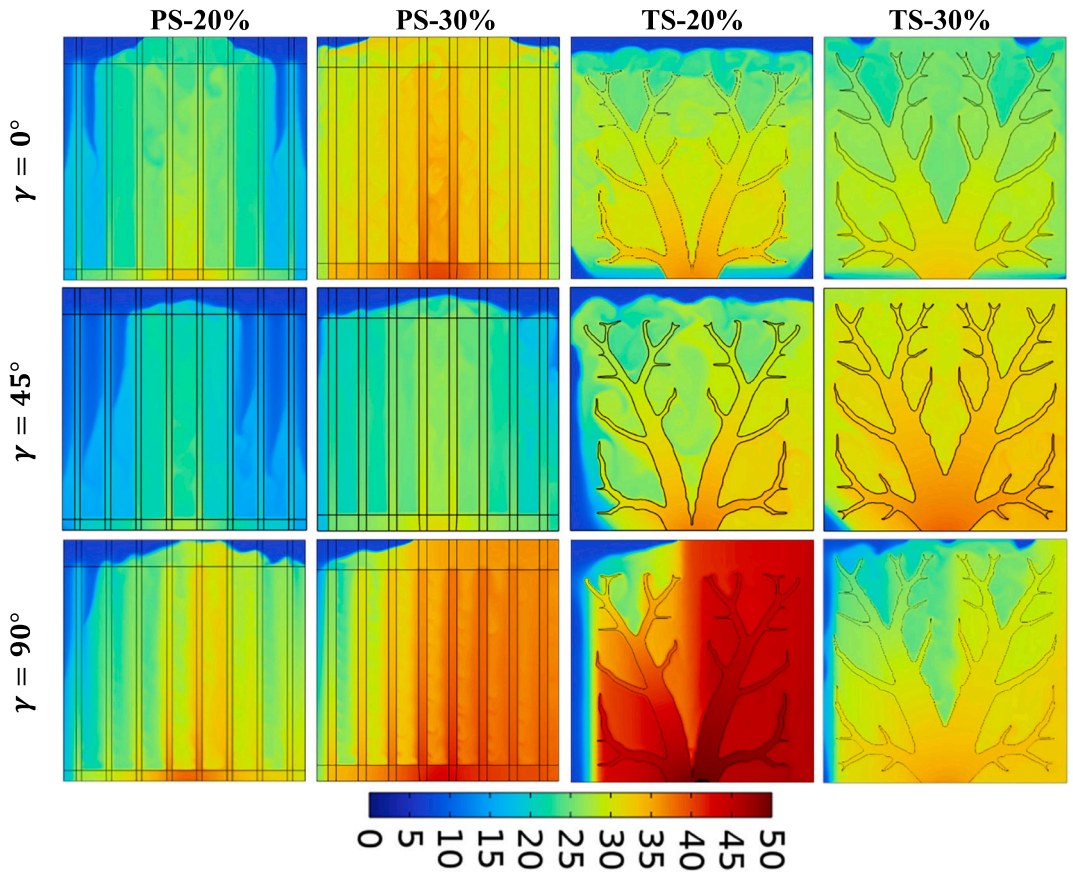

Fig. 15. Isotherms for $(\theta - \theta_c)$ at various inclination angles at $t = 2400\ s$. Temperature higher than $50^{\circ}C$ is depicted the same as $50^{\circ}C$.

Table 3
The melting time ($(MT\ (s))$ for charging states of $MVF = 0.75$ and $MVF = 1.0$.

Angle	PS-20 %		TS-20 %		PS-30 %		TS-30 %	
	MVF = 0.75	MVF = 1.0	MVF = 0.75	MVF = 1.0	MVF = 0.75	MVF = 1.0	MVF = 0.75	MVF = 1.0
0°	1865	**2803**[a]	1915	**2750**	1608	**2468**	1650	**2387**
15°	1875	2809	1925	2860	1609	2475	1650	2399
30°	2100	3394	1925	3067	1609	2472	1650	2401
45°	2100	3396	1925	3246	1765	2995	1650	2417
60°	2075	3328	1925	3358	1609	2517	1650	2456
75°	2025	3212	1935	3506	1609	2549	1655	2538
90°	1795	2925	1950	3449	1610	2655	1655	2585

[a] The shortest full melting time is bolded.

4. Results and discussion

4.1. Examining the impact of fin structure on heat source maximum temperature, MVF, and fin temperature distribution

Fig. 8(a) demonstrates that the PCM's melting process can be classified into three well-defined steps, determined by the changes in the maximum temperature of the heat source: (1) the warm-up step, (2) the first or main step of PCM melting, and (3) the second step of PCM melting. In the initial step, there is a significant and rapid rise in the maximum temperature of the heat source over a relatively short duration ($t < 80s$). As Fig. 8(b) presents, the PCM melting does not commence during this particular step. Consequently, the heat primarily undergoes conduction and is predominantly stored as sensible heat within the phase change substance and fins. When the heating process advances, the heat transfer moves into the primary melting step of the PCM. In this step, the rate of temperature increase in the heat source decelerates because of the relatively rapid melting rate of the PCM. During the secondary melting step, when the majority of the PCM has undergone liquefaction, the rate of PCM melting decreases. At the same time, the heat source temperature experiences a rapid increase due to the resurgence of conduction heat transfer as the primary influencing factor.

During the initial phase of the main step in the melting process, heat sinks equipped with tree-shaped fins demonstrate superior performance compared to those with plate fins in achieving lower heat source temperatures. This phenomenon can be attributed to the enhanced heat diffusion facilitated by the tree-shaped structure, which allows the heat source to transfer its heat into the PCM region more effectively. Consequently, the initiation of PCM melting can occur at multiple locations, causing a decrease in the temperature of the heat source.

At the end of the melting process, for the structure with a volume fraction of 20 %, the optimized structure shows a higher temperature for the hot source compared to the container with the plate fins. However, when the structure has a volume fraction of 30 %, the topologically optimized structure exhibits a lower temperature. Additionally, the

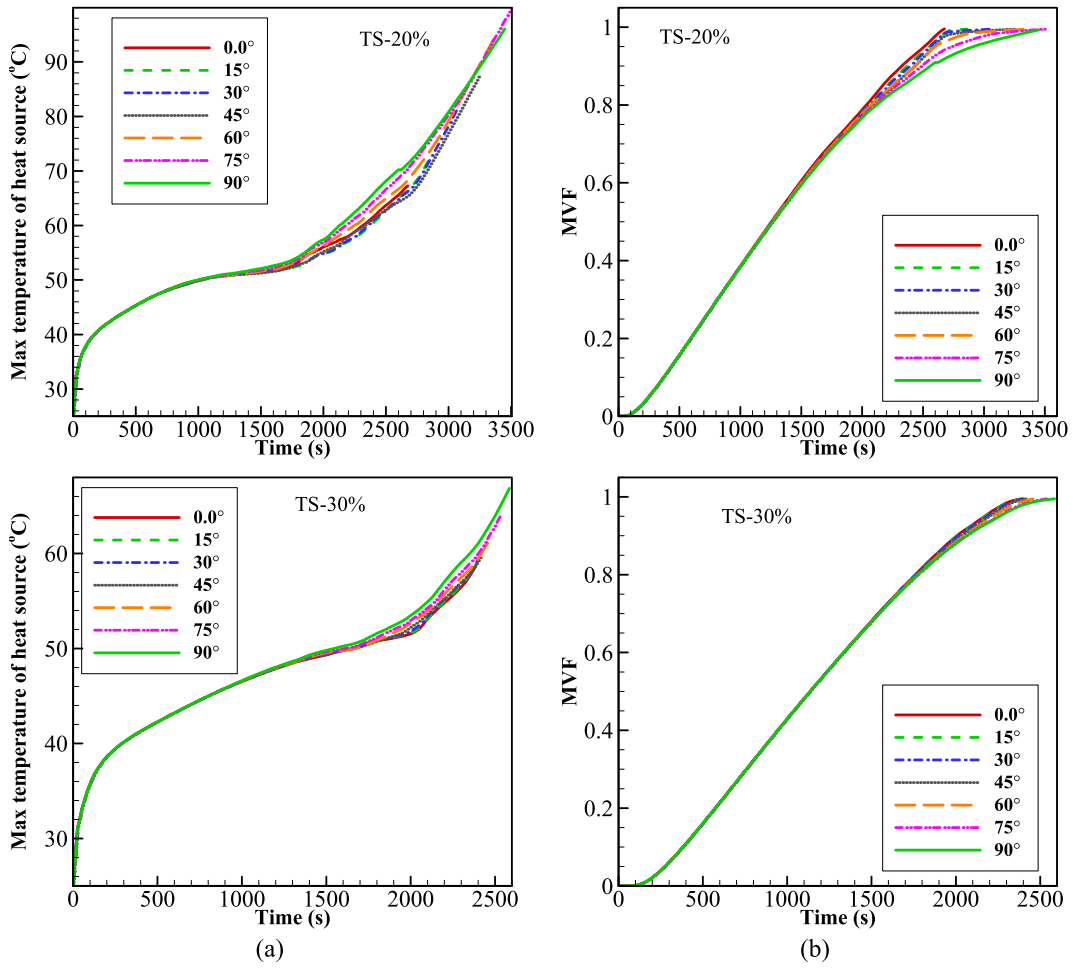

Fig. 16. Effect of inclination angle on (a) the maximum temperature of heat source of heat sinks, and (b) the melted volume fraction inside the heat sinks with different configurations of fins.

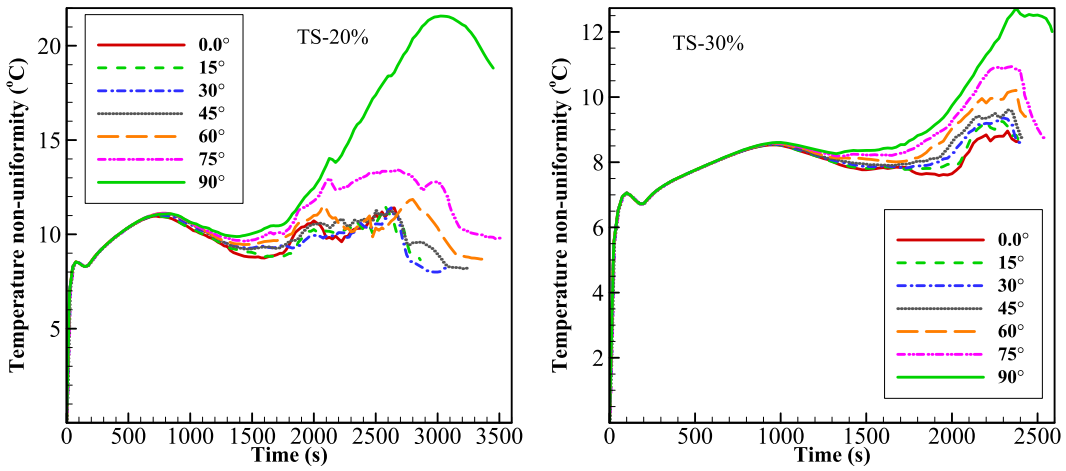

Fig. 17. Temperature non-uniformity of the tree-shaped fins with different inclination angles of the heat sink.

results demonstrate that the heat sinks with the tree-shaped design of fin perform more effectively in achieving higher melting fractions (Fig. 8 (b)).

To examine the heat dissipation efficiency of various metal structures, the non-uniformity of the fin temperature is assessed. The non-uniformity is quantified as the temperature disparity between the highest and lowest temperatures experienced by the fin. A diminished temperature non-uniformity suggests enhanced heat dispersion effectiveness, reduced risk of heat source overheating, and ensures a more homogeneous melting process. As depicted in Fig. 9, the temperature non-uniformity of the structures having the topological design is noticeably lower than that observed in the plate fins. This inference implies that utilizing the topological optimization method to enhance heat diffusion within the PCM container is proving to be successful.

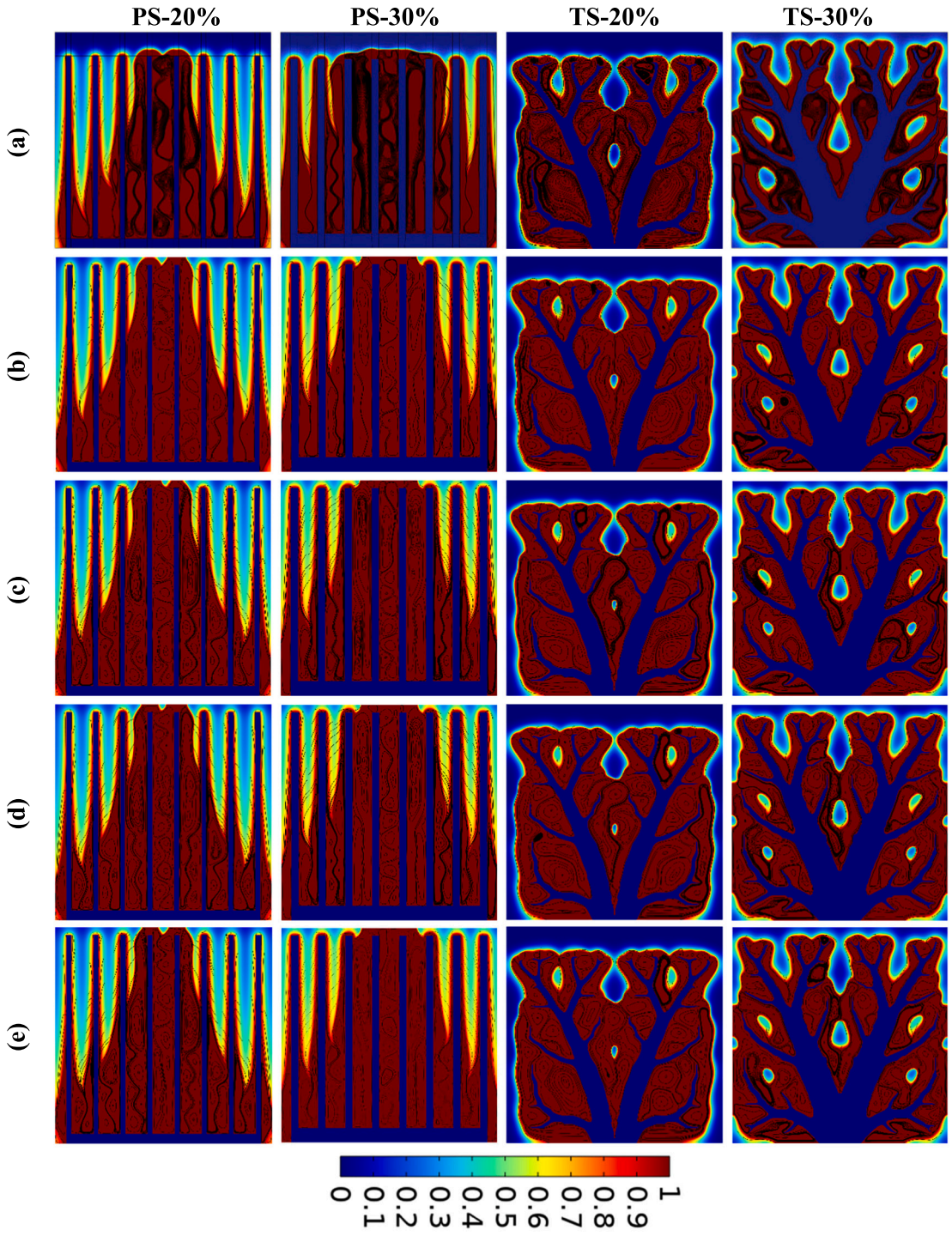

Fig. 18. Phase change interface and streamlines for different designs of heat sink occupied with various NePCMs at $t = 1800\ s$: (a) pure PCM, (b) NePCM containing Cu nanoparticles, (c) NePCM containing GO nanoparticles, (d) NePCM containing MWCNTs, and (e) NePCM containing Al_2O_3.

4.2. Exploring the influence of fin structure on melting field, streamlines, and isotherms

To gain deeper insights into the influence of fin topology on the thermal behavior of PCM, Figs. 10 and 11 display the fields of melting, streamlines, and temperature over time, encompassing both the main and second steps of melting PCM. It is worth noting that the inclination angle of the heat sink is 45°. These visualizations provide a comprehensive understanding of the thermal processes involved in the system. Fig. 10 illustrates that heat sinks equipped with plate fins demonstrate a distinct thermal response. The heat source initiates the melting of the adjacent solid PCM, predominantly initiating along the plate fin walls. The temperature distribution within the metal fins predominantly influences this phenomenon. Over time, the lower regions of the enclosure foster the emergence of minute vortices within the heat sink channels. Subsequently, these vortexes gradually increase in size and ascend along the plates throughout the phase change duration, finally encompassing the entire length of the PCM channel. Previous reports have indicated that a larger vortex can lead to improved temperature mixing, thereby enhancing the melting process of PCM [42].

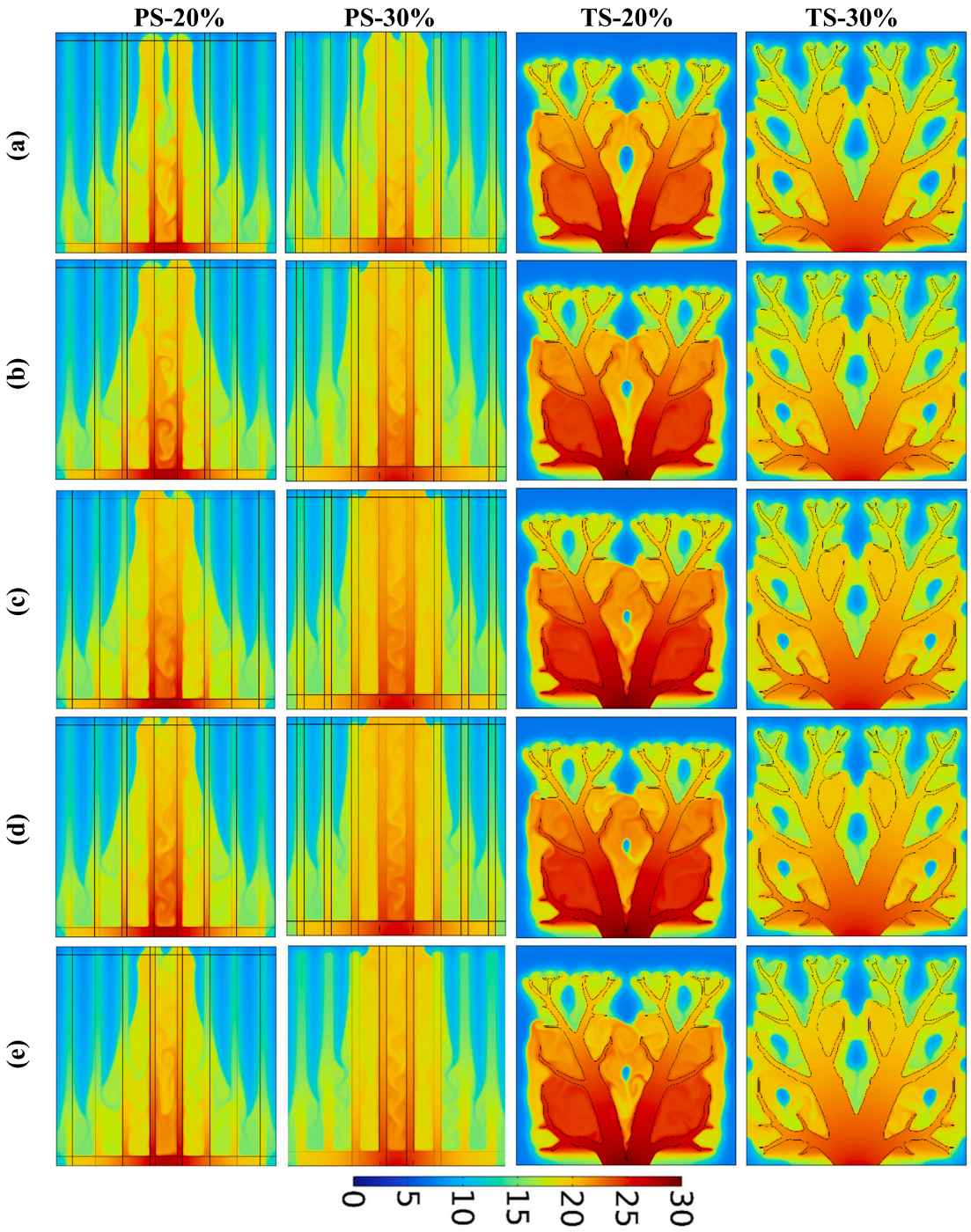

Fig. 19. Temperature fields for different designs of heat sink occupied with various NePCMs at $t = 1800\ s$: (a) pure PCM, (b) NePCM containing Cu nanoparticles, (c) NePCM containing GO nanoparticles, (d) NePCM containing MWCNTs, and (e) NePCM containing Al_2O_3.

In contrast to the containers having plate fins, the melting fronts in the heat sink with tree-shaped fins exhibit greater complexity, as illustrated in Fig. 10. The presence of curvilinear branches of the tree-shaped fins in the heat sink results in a significantly higher number of vortexes than the heat sink with plate fin designs. Consequently, it is expected that advection heat transfer will be improved. This finding can visually be seen in Fig. 8(b).

To enhance our comprehension of how the fin configurations influences the temperature distribution inside the PCM domain, it is presented a series of temperature contour plots within the heat sink occupied by PCM at various time points. The results are depicted in Fig. 11. By increasing the volume fraction of the fins, we can significantly reduce the temperature non-uniformity in the PCM container. This improvement is a direct consequence of the enhanced overall thermal conductivity within the PCM containers, which is achieved through the greater proportion of metal in the mixture.

4.3. Investigating the impact of heat sink inclination angles and diverse fin structures on the melting and temperature fields, heat source maximum temperature, MVF, and fin temperature distribution

The influence of the inclination angle of the heat sink on the melting and temperature fields at two specific time points, namely $t = 1200\ s$ and $t = 2400\ s$, is examined in Figs. 12–15. As anticipated, when the

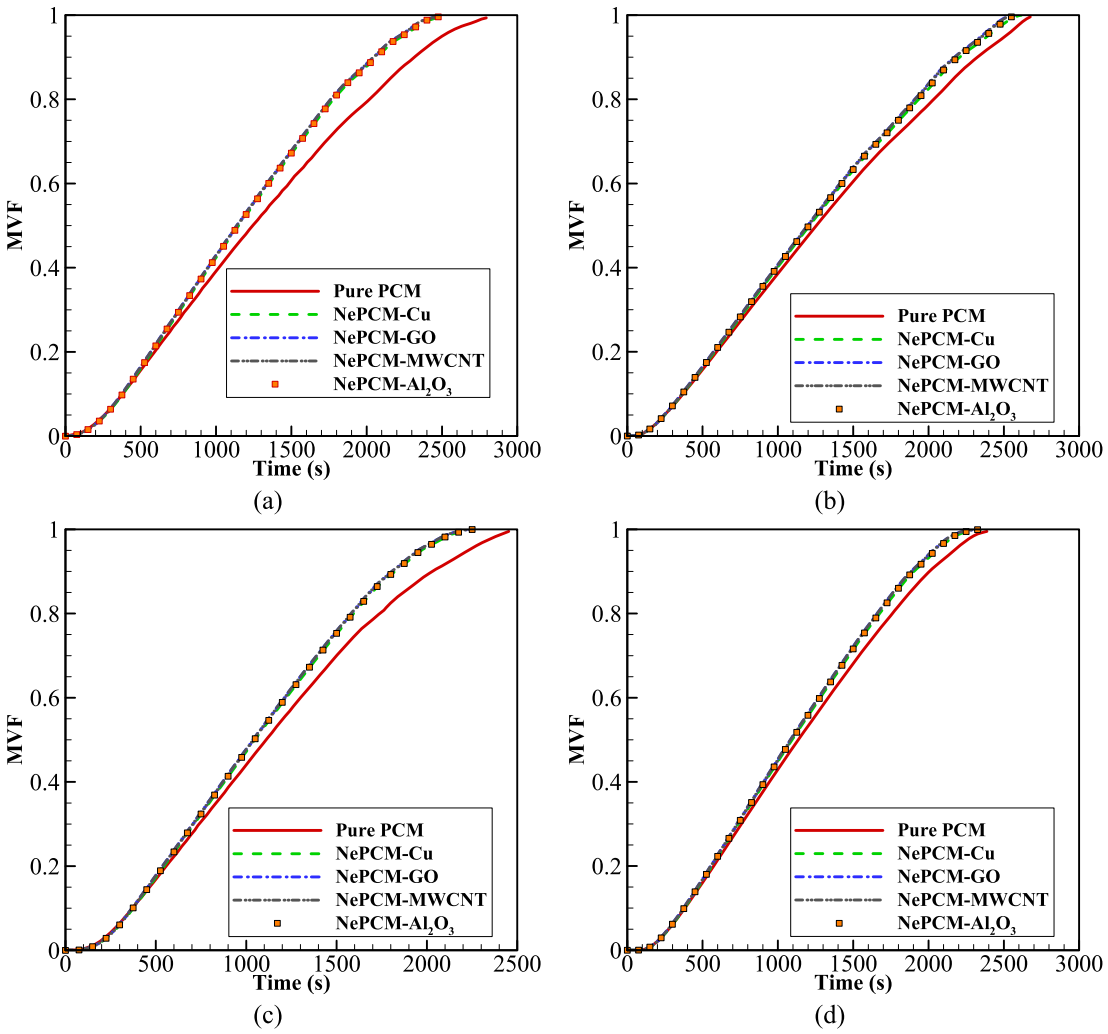

Fig. 20. The volume fraction of NePCM containing a 5 % volume fraction of various nanoparticles for (a) PS-20 %, (b) TS-20 %, (c) PS-30 %, and (d) TS-30 %.

Table 4
The melting time (MT (s)), maximum temperature of heat source ($T_{max}(^{\circ}C)$), and temperature non-uniformity ($\Delta T_{max}(^{\circ}C)$) of the NePCM containing a 5 % volume fraction of various nanoparticles for different designs of heat sink.

NP[a]	PS-20 %			TS-20 %			PS-30 %			TS-30 %		
	MT	T_{max}	ΔT_{max}	MT	T_{max}	ΔT_{max}	MT	T_{max}	ΔT_{max}	MT	T_{max}	ΔT_{max}
PP[b]	2803	66.97	12.84	2750	67.28	10.94	2468	67.22	9.90	2387	58.76	8.63
Cu[c]	2517	66.10	15.64	2615	67.80	12.12	2258	60.46	11.51	2346	61.45	8.99
GO[d]	2482	66.10	15.57	2562	67.50	11.90	2231	60.52	11.42	2310	61.54	8.69
MWCNT[e]	2485	66.24	15.58	2569	67.96	11.41	2233	60.65	11.42	2310	61.47	8.63
Al_2O_3[f]	2509	65.89	15.47	2594	67.62	11.94	2252	60.41	11.39	2335	61.33	9.16

[a] Nanoparticles.
[b] Pure PCM.
[c] Copper nanoparticles.
[d] Graphene oxide.
[e] Multi-wall carbon nanotubes.
[f] Aluminum oxide.

inclination angle is set at 0°, the governing fields exhibit symmetry. At $t = 1200\ s$, under the inclination angles of 45° and 90°, the PCM adjacent to the heat sources in the plate heat sinks melts asymmetrically and the molten liquid ascends in the direction of the heat sources. This phenomenon is attributed to the buoyancy force induced by gravity acting on the molten liquid. Nevertheless, it is evident that at $t = 1200\ s$, the PCM in the tree-shaped heat sinks experiences an almost symmetric melting. This observation indicates that in tree-shaped heat sinks, the buoyancy force has a relatively small effect, and the melting process is primarily driven by the influence of the thermal conduction mechanism. Furthermore, Fig. 13 illustrates that at $t = 2400\ s$, under inclination angles of 45° and 90°, the buoyancy force induces a greater degree of melting in the PCM within the right-hand region of the heat sinks. Additionally, the inclination angle exerts the most significant influence on the tree-shaped heat sink with the metal volume fraction of 20 %.

As depicted in Figs. 14 and 15, the temperature fields align with the

melting patterns, indicating that the areas where the PCM undergoes melting exhibit higher temperatures compared to the regions with the solid PCM. Moreover, it is found that the temperature non-uniformity in the tree-shaped heat sink with a metal volume fraction of 20 % is more significantly influenced by the inclination angle. This is due to that the PCM in the right-hand portion of the heat sink is earlier melted, and after that, the heat transferred through the metal structure increases the temperature of molten liquid. This phenomenon is because the PCM in the right-hand portion of the heat sink undergoes earlier melting. Subsequently, the heat transferred through the metal structure elevates the temperature of the molten liquid in this region. However, the heat reaching the left side of the heatsink is employed to melt the PCM at a relatively constant temperature.

Table 3 shows the melting time (in seconds) for the charging states of $MVF = 0.75$ and $MVF = 1.0$ for heat sinks with various fin shapes. The results clearly demonstrate that the heat sink with $\gamma = 0.0^{\circ}$ achieves the shortest complete phase change time. The underlying reason behind this observation is that at a tilt angle $\gamma = 0.0^{\circ}$, the buoyancy forces exert the most significant influence on the convection of the melted PCM. Consequently, the mixing of the molten liquid reaches its maximum level at this particular angle. Fig. 16(a) further supports this finding. Furthermore, Table 3 demonstrates that the heat sink with tree-shaped design fins and a volume fraction of 30 % exhibits the least dependency of the melting time on the inclination angle. Meanwhile, the thermal behavior of the heat sink of PS-20 % is the most sensitive to the tilt angle. This finding highlights the varying sensitivities of different fin configurations to changes in the tilt angle and emphasizes the superior thermal stability of the tree-shaped heat sink at a 30 % volume fraction. Furthermore, the results indicate that for $\gamma = 75^{\circ}$ and 90°, the complete phase change time of the PCM in the heat sink with TS-20 % is significantly longer compared to the heat sink with PS-20 %. Nonetheless, the full phase change time of the tree-shaped and plate designs does not exhibit a significant difference at the other tilt angles.

Fig. 16(b) illustrates the varying maximum temperature of the concentrated heat source with TS-20 % and 30 % for different inclination angles of the heat sink. As depicted, when $t < 1800s$, the tilting of the heatsink does not appear to have any significant impact on the behavior of the maximum temperature. At this stage, the melting process is primarily governed by thermal conductivity, and convection does not play a significant role. Consequently, the tilting of the heatsink has minimal impact on the maximum temperature. Following this stage, during the secondary melting stage, it is observed that the heat sink with $\gamma = 90^{\circ}$ exhibits the highest temperature for the hot source. Exactly, during this stage, the heat sink with a $\gamma = 90^{\circ}$ experiences a minimal melting rate of the PCM. Consequently, a reduced amount of heat is transmitted from the heat source by the fin to the PCM in this particular configuration. As a result, the heat source's temperature remains comparatively higher compared to other tilt angles.

Dependency of the temperature non-uniformity in the tree-shaped fins on the inclination angle is illustrated in Fig. 17. It is worth noting that temperature non-uniformity is defined as the disparity between the maximum and minimum temperatures experienced by the fin, i.e., $(\theta_{max,fin} - \theta_{min,fin})$. As depicted in the figures, both configurations exhibit the highest temperature non-uniformity when the heat sink has a 90° inclination angle. Meanwhile, the heat sink with $\gamma = 0.0^{\circ}$ results in the most favorable temperature uniformity within the fin.

4.4. Thermal performance evaluation of different NePCMs in diverse heat sink designs

This section addresses the influence of diverse nanoparticles dispersed within the PCM on the thermal performance of various heat sink designs with the inclination angle of $\gamma = 0.0^{\circ}$. The relations used to provide the thermophysical properties of NePCMs can be found in [43]. The nanoparticles dispersed in the PCM encompass copper nanoparticles (Cu), graphite oxide nanoparticles (GO), multi-walled carbon nanotubes (MWCNT), and aluminum oxide nanoparticles (Al_2O_3). The thermophysical properties of these nano-additives are detailed in [44–46]. Figs. 18 and 19 illustrate the melting and temperature fields of various heat sinks filled with distinct NePCMs when $t = 1800\,s$. It is worth noting that the volume fraction of the dispersed nanoparticles in the pure PCM is maintained at 5 %. As evident from these figures, the incorporation of various types of nanoparticles into the pure fluid results in an improvement in the melting rate. This can be attributed to the increase in the effective thermal conductivity of the PCM. As depicted in Figs. 18–20, no significant differences can be discerned in the phase change interface, temperature fields, and MVF among the various NePCMs. Furthermore, the study reveals that the impact of nanoparticles on enhancing the melting rate is more pronounced in the plate-fin heat sinks. This fact is visually depicted in Fig. 20, and further quantitative details can be found in Table 4, presenting the relevant data.

The outcomes illustrated in Table 4 indicate that the increase in melting rate attributed to the presence of diverse nanoparticles is more pronounced for plate-fin heat sinks in comparison to tree-shaped heat sinks. Additionally, it is observed that dispersing the nano-additives into the PCM results in the plate-fin heat sink-20 % showing the most significant increase in melting rate. Conversely, the tree-shaped heat sink-30 % exhibits the least enhancement. Moreover, with the addition of nano-particles to the PCM, there is not a substantial variation in the maximum temperature of the concentrated heat source (T_{max}) for PS-20 %, TS-20 %, and TS-30 %. In contrast, the dispersion of various nano-additives in the PCM within PS-30 % leads to a significant decrease in T_{max} (a nearly $6.5^{\circ}C$ reduction is evident.). The findings also illustrate that the presence of nanoparticles can intensify the temperature non-uniformity (ΔT_{max}) within the metal structures. Finally, as tabulated, the most significant intensification in ΔT_{max} with the nanoparticles is observed for PS-20 %. However, TS-30 % exhibits the least increase in temperature non-uniformity within the metal structure.

5. Conclusion

This research presents a heat control remedy for an electronic gadget by utilizing a specific PCM. A slanted receptacle containing PCM based on paraffin wax is suggested as a means to capture the heat emitted by the concentrated heat origin. Two arrangements of plate fins, with volume proportions of 20 % and 30 % across the complete container, are under examination. In order to improve heat dispersion, a density-driven topology optimization technique formulated by Liu and Tovar [33] is utilized. Using tree-shaped topological optimization methodologies, this approach rearranges the pathway of heat conduction, redirecting it from the heat origin to the designated PCM area.

- The phase-change process of the PCM is clearly characterized by three distinct steps, delineated by variations in the maximum temperature of the heat source. These steps include (1) the warm-up step, (2) the primary step of phase-change process, and (3) the secondary step of phase-change process. During the warm-up and secondary phases of PCM melting, the dominant heat transfer mechanism was conduction. This resulted in a rapid increase in the temperature of the heat source. During the initial phase of the phase-change process, the rate of PCM melting was expedited as a result of the heightened convection flow occurring within the liquefied PCM. Consequently, the heat source temperature exhibited a gradual increase during this phase.
- At the beginning of the first melting stage, heat sinks featuring tree-shaped fins outperform those with plate fins in achieving lower temperatures for the heat source. Nevertheless, beyond that stage, plate fins prove to be more effective in maintaining lower temperatures for the heat source. Moreover, structures utilizing the

topological design exhibited significantly lower temperature non-uniformity than those equipped with plate fins.

- The study's findings offer compelling evidence that heat sinks with different configurations (plate or tree-shaped design) and an inclination angle of $\gamma = 0^{\circ}$ achieve the fastest complete melting time. At inclination angles of $\gamma = 75^{\circ}$ and 90°, the incorporation of a tree-shaped fin design into the heat sink, constituting 20 % of the total volume, yields an extended period for the complete melting of the PCM as compared to the heat sink featuring a plate design. Nevertheless, when considering alternative tilt angles, there is no noteworthy contrast in the time taken for complete melting between the configurations employing tree-shaped and plate designs.
- The results reveal a more pronounced increase in melting rate due to the presence of diverse nanoparticles for plate-fin heat sinks compared to tree-shaped heat sinks. Additionally, when dispersing nano-additives into the phase change material (PCM), the plate-fin heat sink with a metal mass fraction of 20 % demonstrates the most substantial enhancement in melting rate, while the tree-shaped heat sink with a metal mass fraction of 30 % shows the least improvement. Furthermore, introducing nano-particles to the PCM does not lead to a substantial variation in the maximum temperature of the concentrated heat source (T_{max}) for PS-20 %, TS-20 %, and TS-30 %. In contrast, the dispersion of various nano-additives in the PCM within PS-30 % results in a significant decrease in T_{max} (with a nearly 6.5 °C reduction observed). The study also highlights that the presence of nanoparticles can amplify temperature non-uniformity (ΔT_{max}) within the metal structures. Finally, the most significant intensification in the temperature non-uniformity within the metal fins with the nano-additives is observed for PS-20 %. However, TS-30 % exhibits the least increase in ΔT_{max}.

As previously mentioned, the existing heat sink design concentrates exclusively on optimizing the heat conduction path within the enhanced structure and accommodating the phase change of the PCM. Moving forward, it would be intriguing to delve into the creation of new heat sinks that consider the impact of natural convection during PCM melting under inclination angles of enclosure as part of the optimization process. Also, topology optimization can be developed to various materials for fin metal structures. Moreover, there is a significant consideration for the use of high-porosity metal foams and matrices in enhancing the performance of electronic devices, ensuring minimal impact on the overall latent heat storage.

CRediT authorship contribution statement

Mohamed Boujelbene: Writing – review & editing, Writing – original draft, Methodology, Conceptualization. **Hakim S. Sultan:** Software, Methodology, Formal analysis, Data curation, Conceptualization. **S.A. M. Mehryan:** Writing – review & editing, Writing – original draft, Validation, Supervision, Investigation, Conceptualization. **Amira M. Hussin:** Investigation, Software, Writing – original draft, Writing – review & editing. **Abed Saif Alghawli:** Investigation, Methodology, Software, Writing – review & editing. **Mohammad Ghalambaz:** Investigation, Methodology, Supervision, Writing – original draft, Writing – review & editing.

Declaration of competing interest

The authors declare that they have no conflict of interest.

Data availability

No data was used for the research described in the article.

Acknowledgments

This study is supported via funding from Prince Sattam bin Abdulaziz University project number (PSAU/2024/R/1445).

References

[1] Z. Zhu, et al., Effect of heat input on interfacial characterization of the butter joint of hot-rolling CP-Ti/Q235 bimetallic sheets by Laser+ CMT, Sci. Rep. 11 (1) (2021) 10020.
[2] Z. Zhu, et al., Investigation into the effect of multiple line dipoles magnetic field through LS-3 parabolic trough solar system, Appl. Therm. Eng. 235 (2023) 121332.
[3] Z. Zhou, et al., Phase change materials for solar thermal energy storage in residential buildings in cold climate, Renew. Sustain. Energy Rev. 48 (2015) 692–703.
[4] E. Saedpanah, M. Lahonian, M.Z. Malek Abad, Optimization of multi-source renewable energy air conditioning systems using a combination of transient simulation, response surface method, and 3E lifespan analysis, Energy 272 (2023) 127200.
[5] F. Agyenim, et al., A review of materials, heat transfer and phase change problem formulation for latent heat thermal energy storage systems (LHTESS), Renew. Sustain. Energy Rev. 14 (2) (2010) 615–628.
[6] N. Mallya, S. Haussener, Buoyancy-driven melting and solidification heat transfer analysis in encapsulated phase change materials, International Journal of Heat and Mass Transfer 164 (2021) 120525.
[7] M.M. Farid, et al., A review on phase change energy storage: materials and applications, Energ. Conver. Manage. 45 (9–10) (2004) 1597–1615.
[8] R. Elarem, et al., A comprehensive review of heat transfer intensification methods for latent heat storage units, Energy Storage 3 (1) (2021) e127.
[9] Z. Khan, Z. Khan, A. Ghafoor, A review of performance enhancement of PCM based latent heat storage system within the context of materials, thermal stability and compatibility, Energ. Conver. Manage. 115 (2016) 132–158.
[10] M. Teggar, et al., Performance enhancement of latent heat storage systems by using extended surfaces and porous materials: a state-of-the-art review, Journal of Energy Storage 44 (2021) 103340.
[11] C. Acar, A comprehensive evaluation of energy storage options for better sustainability, Int. J. Energy Res. 42 (12) (2018) 3732–3746.
[12] F. Farzaneh, S. Jung, Experimental and numerical investigation on enhancing capped-end tube energy absorption capacity by orifice effect, Structures 53 (2023) 1450–1462.
[13] F.U. Hasnain, Numerical Study to Enhance the Melting and Solidification of Phase Change Material Using Branched Fins and Nano-Particles, Capital University, 2020.
[14] Z. Badiei, M. Eslami, K. Jafarpur, Performance improvements in solar flat plate collectors by integrating with phase change materials and fins: a CFD modeling, Energy 192 (2020) 116719.
[15] R. Karami, B. Kamkari, Investigation of the effect of inclination angle on the melting enhancement of phase change material in finned latent heat thermal storage units, Appl. Therm. Eng. 146 (2019) 45–60.
[16] P.H. Biwole, et al., Influence of fin size and distribution on solid-liquid phase change in a rectangular enclosure, Int. J. Therm. Sci. 124 (2018) 433–446.
[17] S. Zhang, et al., Comparative study on heat transfer enhancement of metal foam and fins in a shell-and-tube latent heat thermal energy storage unit, Energy Storage and Saving 2 (2023) 487–494.
[18] M. Mahdavi, S. Tiari, V. Pawar, A numerical study on the combined effect of dispersed nanoparticles and embedded heat pipes on melting and solidification of a shell and tube latent heat thermal energy storage system, Journal of Energy Storage 27 (2020) 101086.
[19] Z.-J. Zheng, et al., Study of the melting performance of shell-and-tube latent heat thermal energy storage unit under the action of rotating finned tube, Journal of Energy Storage 62 (2023) 106801.
[20] W.-W. Wang, L.-B. Wang, Y.-L. He, Parameter effect of a phase change thermal energy storage unit with one shell and one finned tube on its energy efficiency ratio and heat storage rate, Appl. Therm. Eng. 93 (2016) 50–60.
[21] C. Li, Q. Li, R. Ge, Assessment on the melting performance of a phase change material based shell and tube thermal energy storage device containing leaf-shaped longitudinal fins, Journal of Energy Storage 60 (2023) 106574.
[22] J. Skaalum, D. Groulx, Heat transfer comparison between branching and non-branching fins in a latent heat energy storage system, International Journal of Thermal Sciences 152 (2020) 106331.
[23] J. Duan, Y. Xiong, D. Yang, Melting behavior of phase change material in honeycomb structures with different geometrical cores, Energies 12 (15) (2019) 2920.
[24] J.Y. Ho, et al., An experimental investigation of a PCM-based heat sink enhanced with a topology-optimized tree-like structure, Energ. Conver. Manage. 245 (2021) 114608.
[25] H. Peng, et al., Discharging process and thermal evaluation in the thermal energy storage system with fractal tree-like fins, Int. J. Heat Mass Transf. 183 (2022) 122073.
[26] J. Xie, et al., Characterization of natural convection in a PCM-based heat sink with novel conductive structures, International Communications in Heat and Mass Transfer 108 (2019) 104306.
[27] C. Zhu, X. Mou, Z. Bao, Optimization of tree-shaped fin structures towards enhanced discharging performance of metal hydride reactor for thermochemical heat storage based on entransy theory, Renew. Energy 220 (2024) 119585.

[28] N.A. Qasem, et al., Influence of tree-shaped fins to enhance thermal storage units, International Communications in Heat and Mass Transfer 151 (2024) 107220.
[29] R. Zhu, D. Jing, Numerical study on the discharging performance of a latent heat thermal energy storage system with fractal tree-shaped convergent fins, Renew. Energy 221 (2024) 119726.
[30] N.B. Khedher, et al., A hybrid solidification enhancement in a latent-heat storage system with nanoparticles, porous foam, and fin-aided foam strips, Journal of Energy Storage 56 (2022) 106070.
[31] J. Xie, et al., Investigations of optimized fin structures in a compact thermal energy storage panel, in: IOP Conference Series: Earth and Environmental Science, IOP Publishing, 2020.
[32] J. Xie, H.M. Lee, J. Xiang, Numerical study of thermally optimized metal structures in a Phase Change Material (PCM) enclosure, Appl. Therm. Eng. 148 (2019) 825–837.
[33] K. Liu, A. Tovar, An efficient 3D topology optimization code written in Matlab, Struct. Multidiscip. Optim. 50 (6) (2014) 1175–1196.
[34] M.P. Bendsoe, O. Sigmund, Topology Optimization: Theory, Methods, and Applications, Springer Science & Business Media, 2003.
[35] T. Gao, et al., Topology optimization of heat conduction problem involving design-dependent heat load effect, Finite Elem. Anal. Des. 44 (14) (2008) 805–813.
[36] M. Saghafian, H. Seyedzadeh, A. Moradmand, Numerical simulation of electroosmotic flow in a rectangular microchannel with use of magnetic and electric fields, Scientia Iranica (2023).
[37] M. Al-Jethelah, et al., Charging nanoparticle enhanced bio-based PCM in open cell metallic foams: an experimental investigation, Appl. Therm. Eng. 148 (2019) 1029–1042.
[38] S.-K. Choi, et al., Computation of the natural convection of nanofluid in a square cavity with homogeneous and nonhomogeneous models, Numer. Heat Transf. A Appl. 65 (4) (2014) 287–301.
[39] J.N. Reddy, D.K. Gartling, The Finite Element Method in Heat Transfer and Fluid Dynamics, CRC Press, 2010.
[40] B. Kamkari, H. Shokouhmand, F. Bruno, Experimental investigation of the effect of inclination angle on convection-driven melting of phase change material in a rectangular enclosure, International Journal of Heat and Mass Transfer 72 (2014) 186–200.
[41] B. Kamkari, H.J. Amlashi, Numerical simulation and experimental verification of constrained melting of phase change material in inclined rectangular enclosures, International Communications in Heat and Mass Transfer 88 (2017) 211–219.
[42] J. Liu, et al., Numerical investigation on the heat transfer enhancement of a latent heat thermal energy storage system with bundled tube structures, Appl. Therm. Eng. 112 (2017) 820–831.
[43] H. Hashemi, Z. Namazian, S.A.M. Mehryan, Cu-water micropolar nanofluid natural convection within a porous enclosure with heat generation, J. Mol. Liq. 236 (2017) 48–60.
[44] S.A.M. Mehryan, et al., Natural convection of magnetic hybrid nanofluid inside a double-porous medium using two-equation energy model, J. Mol. Liq. 277 (2019) 959–970.
[45] M. Ghalambaz, et al., Melting process of the nano-enhanced phase change material (NePCM) in an optimized design of shell and tube thermal energy storage (TES): Taguchi optimization approach, Appl. Therm. Eng. 193 (2021) 116945.
[46] S.A.M. Mehryan, et al., Free convection of hybrid Al2O3-Cu water nanofluid in a differentially heated porous cavity, Adv. Powder Technol. 28 (9) (2017) 2295–2305.